isvr Institute of Sound and Vibration Research

Three-dimensional Elastodynamic Analysis Using Multiple Boundary Element Domains

L. Andersen and C.J.C. Jones

ISVR Technical Memorandum 867

October 2001

University of Southampton

SCIENTIFIC PUBLICATIONS BY THE ISVR

Technical Reports are published to promote timely dissemination of research results by ISVR personnel. This medium permits more detailed presentation than is usually acceptable for scientific journals. Responsibility for both the content and any opinions expressed rests entirely with the author(s).

Technical Memoranda are produced to enable the early or preliminary release of information by ISVR personnel where such release is deemed to the appropriate. Information contained in these memoranda may be incomplete, or form part of a continuing programme; this should be borne in mind when using or quoting from these documents.

Contract Reports are produced to record the results of scientific work carried out for sponsors, under contract. The ISVR treats these reports as confidential to sponsors and does not make them available for general circulation. Individual sponsors may, however, authorize subsequent release of the material.

UNIVERSITY OF SOUTHAMPTON
INSTITUTE OF SOUND AND VIBRATION RESEARCH
DYNAMICS GROUP

Three-Dimensional Elastodynamic Analysis Using Multiple Boundary Element Domains

By

L. Andersen and C.J.C. Jones

ISVR Technical Memorandum No. 867

October 2001

Authorized for issue by
Dr. M.J. Brennan
Group Chairman

Summary

The report describes the theory for three-dimensional boundary element analysis of viscoelastic media in the frequency domain. Quadrilateral and triangular elements with quadratic interpolation are used in the discretization. A model is developed which may be used for the analysis of a structure consisting of several open or closed boundary element sub-domains. Furthermore, the method allows for a simple coupling method to a finite element scheme. The method outlined in the present report forms the theoretical basis for the boundary element program BEASTS, the documentation for which may be found in Reference [2].

For the analysis of structures or layered ground with a single plane of symmetry, a method for reducing the mesh, making use of the geometry, is developed. Finally numerical examples are given for a homogeneous and a layered half-space. The results from the boundary element scheme are checked against a semi-analytical solution, and especially the effects of the truncation of the boundaries are investigated. The boundary element scheme is found to provide satisfactory results when only three elements are used per wavelength, and the local behaviour at a loading point is well described, even when the mesh ends less than a single wavelength away from the source.

Contents

Glossary of Symbols

Greek Symbols

Γ	Surface of domain for BE formulation
Γ_j	Surface of boundary element j
Γ_p	Part of boundary where non-zero traction is applied
Δ	Dilation
Σ^*_{ijl}	Component i,j,l in the Green's function for the stress in the frequency domain
$\mathbf{\Phi}_j$	Shape function matrix for element j
Φ_l	Scalar field for load applied in coordinate direction l in Helmholz decomposition of load field
Ψ_{il}	Vector field for load applied in coordinate direction l in Helmholz decomposition of load field
Ω	Domain for BE formulation
α, β	Terms of the displacement Green's function
δ_{ij}	Kronecker's delta
$\delta\mathbf{u}$	Virtual displacement field vector
$\delta\mathbf{u}_j$	Virtual nodal displacements for element j
$\delta\mathbf{p}$	Surface traction vector
δw	Virtual work
δw_j	Virtual work on the surface of element j
ϵ_{ij}	Component i,j of the infinitesimal strain tensor
ν	Poisson ratio
λ, μ	Lamé constants for a homogeneous isotropic elastic medium
ξ_1, ξ_2	Homogeneous element coordinates
ξ_3	Third homogeneous coordinate for triangular elements
ρ	Mass density
σ_{ij}	Component i,j of the Cauchy stress tensor

ϕ_i Shape function for node i of an element

φ_l Scalar field for load applied in coordinate direction l in Helmholz decomposition of displacement field

ψ_{il} Vector field for load applied in coordinate direction l in Helmholz decomposition of displacement field

ω Circular frequency

Latin Symbols

B_i Component i of the load per unit mass in the frequency domain

B^*_{ij} Component i,j of the unit amplitude harmonically varying load in the frequency domain

$\hat{\mathbf{C}}$ Matrix with geometry constants for an entire BE domain

C_{il} Component i,l of the geometric constant tensor for a collocation point

E Young's modulus

$\mathbf{F}_j$ Nodal force amplitudes for degrees of freedom in element j

$\mathbf{G}$ Square displacement Green's function matrix for an entire BE domain

$\hat{\mathbf{G}}$ Non-square displacement Green's function matrix for an entire BE domain

$\mathbf{G}_{ibed}$ Square displacement Green's function matrix for BE domain *ibed*

$\mathbf{H}$ Sum of traction Green's function matrix and geometric constants matrix for an entire domain

$\hat{\mathbf{H}}$ Traction Green's function matrix for an entire domain

$\mathbf{H}_{ibed}$ Sum of traction Green's function matrix and geometric constants matrix for BE domain *ibed*

$\mathbf{J}$ Jacobian

$\mathbf{K}_{ibed}$ Equivalent FE stiffness matrix for BE domain *ibed*

N Number collocation nodes in a BE domain

N' Number of columns in non-square displacement Green's function matrix for an entire BE domain

N_B Number of degrees of freedom in boundary element domain

N_F	Number of degrees of freedom in finite element domain
N_j	Number of nodes in element j
NE	Number of integration element in a BE domain
$\mathbf{P}^*$	Traction Green's function matrix for a collocation node
$\mathbf{P}_{ibed}$	Nodal displacements for BE domain *ibed*
P_i	Component i of the surface traction
P^*_{il}	Component i,l in the Green's function for the surface traction in the frequency domain
$\mathbf{P}_j$	Nodal traction amplitudes for element j
$\mathbf{T}_{ibed}$	Transformation matrix for BE domain *ibed*
$\mathbf{U}^*$	Displacement Green's function matrix for a collocation node
U_i	Component i of the displacement field in the frequency domain
$\mathbf{U}_{ibed}$	Nodal tractions for BE domain *ibed*
U^*_{il}	Component i,l of the Green's function for displacement in the frequency domain
$\mathbf{U}_j$	Displacements for all degrees of freedom in a boundary element
b_i	Component i of the load per unit mass in the time domain
c_g	Group (energy) velocity of waves
c_P	Phase velocity of pressure waves
c_S	Phase velocity of shear waves
e_{ijk}	Permutation symbol
f	Frequency
$\mathbf{f}_j$	Nodal force vector for degrees of freedom in element j
k_P	Wave number for pressure waves
k_S	Wave number for shear waves
l	Index used solely to indicate the direction of the load in the Green's functions
$\mathbf{n}$	Outward unit normal vector
$\mathbf{p}_j$	Nodal tractions for element j

p_j	Component j of the surface traction
r	Distance between the observation point and the source point
t	Time
$\mathbf{u}$	Displacement field vector
u_i	Component i of the displacement field in the time domain
$\mathbf{x}$	Position vector to observation point
$\mathbf{x}_i$	Coordinate vector for collocation node i
x_i	Component i of the position vector $\mathbf{x}$
$\mathbf{y}$	Position vector to source point
y_i	Component i of the position vector $\mathbf{y}$

1 Introduction

For a homogeneous or a layered half-space with horizontal surface and interfaces an analytical solution may be derived for the response due to excitation on the surface or within the ground. However, for structures/layered ground with complicated geometries, such as a bored or cut-and-cover tunnel, the need arises for a numerical solution. In the case of structures and media of (semi) infinite extent, the boundary element method is a powerful tool due to its inherent capability to model radiating waves. Thus it is particularly useful for the analysis of submerged railway structures, which are the primary concern in the present project.

A variety of problems may be analysed using a two-dimensional model. For the examination of the wave propagation due to a line load in *e.g.* a railway tunnel, a boundary element program was developed in References [5, 7, 6]. However, when point forces, or sources that are otherwise confined to a limited space, are applied, a three-dimensional boundary element scheme has to be used - even if the geometry of the structure is two-dimensional as is often the case in railway engineering. The present project deals with the formulation of a boundary element (BE) scheme, which may be used for the analysis of wave propagation through the ground due to harmonically varying excitation in a railway tunnel. Ground borne noise has a dominant frequency range of about 30 Hz to 160 Hz. However, vibration that is perceptible as 'whole body vibration' has a nominal upper frequency limit of 80 Hz. The objective is to develop a BE model capable of dealing with three-dimensional wave propagation problems in this frequency range with reasonable computing resources.

With the computing resources available, elements with lower order interpolation (*i.e.* constant or linear elements) are inadequate for the discretization for this frequency range since the rate of convergence is very slow. Thus an immense amount of degrees of freedom are needed at high frequencies to obtain satisfactory results. On the contrary only 3-4 elements $\sim$ 6-8 nodes per wave length are found to be sufficient when quadratic interpolation is used. Therefore nine-noded quadrilateral elements and six-noded triangular elements are used in the present work.

A method for coupling several BE sub-domains, and possibly also BE domains with finite elements, is described. Different coupling techniques are considered where either surface tractions are transformed into nodal forces (in a finite element sense) or nodal forces are interpreted as surface tractions (in the boundary element sense). For reasons given in Section 3, it has been chosen to transform each boundary element into a macro element, thus performing the coupling in the finite element way.

The theory explained in this report has been implemented in a suite of computer programs entitled BEASTS (Boundary Element Analysis of Soil and Three-dimensional Structures). A further description of the software may be found in Reference [2]. In the documentation of the software, numerical examples are given of wave propagation due to a stationary, harmonically-varying point source in a bored tunnel. In this report examples are given of wave propagation due to excitation on the surface of a homogeneous or layered half-space and comparisons are made with a semi-analytical solution and a BE scheme using the original surface traction approach.

2 Formulation of a Boundary Element Domain

The first step in establishing a multi-domain boundary element model is to have a model for a single BE domain. For this purpose the formulation of a BE domain is given in this section.

2.1 Outline of Boundary Element Method Theory

Consider an elastic body Ω which has the surface Γ with outward unit normal vector $\mathbf{n}$, see Figure 1. The basic idea of the boundary element method (BEM) for elastidynamics is to establish a relationship between the known and unknown values of the displacement and the surface traction on the boundary. To achieve this, a discretization and numerical integration only has to be performed over the surface Γ, not over the entire domain Ω. This reduces the spatial dimension of the integration by one when compared to the finite element method (FEM).

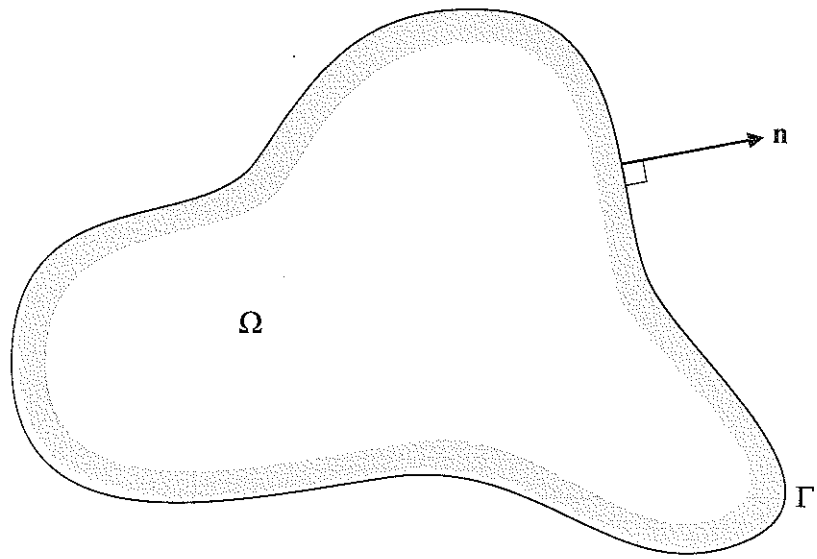

Figure 1. The domain Ω with surface Γ and outward unit normal $\mathbf{n}$.

The fundamental equation in the elastodynamic BEM is the boundary integral equation known as Somigliana's identity. This equation, which is derived from the Betti reciprocal theorem, uses the Green's functions as weighting functions. Since the Green's functions automatically satisfy the Sommerfeld radiation condition, the BEM is especially well-suited to problems involving exterior domains, *e.g.* layered or homogeneous soil.

The following subsection describes how the Green's function for an elastic, homogeneous and isotropic continuum is derived for dynamic analysis in the frequency domain. Subsequently, in Subsections 2.2 to 2.5, the different steps in the discretization and intergration process are described. Finally, a discussion of how to model more complicated structures than is possible with a single BE domain is to be found in Subsection 2.6.

2.2 Derivation of the Frequency Domain Full-Space Green's Functions

In Cartesian coordinates, x_j, the time domain equation of motion for an isotropic, homogeneous viscoelastic medium with mass density ρ may be written,

$$\frac{\partial}{\partial x_j}\sigma_{ij}(\mathbf{x},t) + \rho b_i(\mathbf{x},t) = \rho\frac{\partial^2}{\partial t^2}u_i(\mathbf{x},t)\,, \tag{1}$$

where $\sigma_{ij}(\mathbf{x},t)$ is the Cauchy stress tensor, $u_i(\mathbf{x},t)$ is the displacement field and $b_i(\mathbf{x},t)$ is the load per unit mass. Vector $\mathbf{x}$ is the position in space and t is the time. The summation convention applies, *i.e.* summation is performed over repeated indices.

Introducing the Lamé constants λ and μ, the stress tensor may be expressed in terms of the dilation, $\Delta(\mathbf{x},t)$, and the infinitesimal strain tensor, $\epsilon_{ij}(\mathbf{x},t)$,

$$\sigma_{ij}(\mathbf{x},t) = \lambda\Delta(\mathbf{x},t)\,\delta_{ij} + 2\mu\epsilon_{ij}(\mathbf{x},t)\,, \tag{2}$$

where δ_{ij} is the Kronecker delta and the following definitions apply,

$$\Delta(\mathbf{x},t) = \frac{\partial}{\partial x_k}u_k(\mathbf{x},t)\,, \quad \epsilon_{ij}(\mathbf{x},t) = \frac{1}{2}\left(\frac{\partial}{\partial x_i}u_j(\mathbf{x},t) + \frac{\partial}{\partial x_j}u_i(\mathbf{x},t)\right). \tag{3}$$

Inserting (2),(3) into (1), the equation of motion in the time domain obtains the form

$$(\lambda+\mu)\frac{\partial^2}{\partial x_i\partial x_j}u_j(\mathbf{x},t) + \mu\frac{\partial^2}{\partial x_j\partial x_j}u_i(\mathbf{x},t) + \rho b_i(\mathbf{x},t) = \rho\frac{\partial^2}{\partial t^2}u_i(\mathbf{x},t)\,. \tag{4}$$

For exitation at a single circular frequency, ω, the components of the load per unit mass may be written $b_i(\mathbf{x},t) = B_i(\mathbf{x},\omega)\,e^{i\omega t}$. Consequently the displacement will also be harmonically varying with time as $u_i(\mathbf{x},t) = U_i(\mathbf{x},\omega)\,e^{i\omega t}$. Hence, in the frequency domain, skipping the exponential time variation terms, the equation of motion becomes,

$$(\lambda+\mu)\frac{\partial^2}{\partial x_i\partial x_j}U_j(\mathbf{x},\omega) + \mu\frac{\partial^2}{\partial x_j\partial x_j}U_i(\mathbf{x},\omega) + \rho B_i(\mathbf{x},\omega) = -\rho\omega^2 U_i(\mathbf{x},\omega)\,. \tag{5}$$

2.2.1 Green's Function for the Displacement Field

The frequency domain Green's function (or fundamental solution) for the displacement, $U^*_{il}(\mathbf{x},\omega;\mathbf{y})$, is the solution to Eq. (5) for a harmonically varying point force with unit amplitude applied at the point $\mathbf{y}$ in the lth direction, that is for a load of the form $\rho B^*_{il}(\mathbf{x},\omega;\mathbf{y}) = \delta(\mathbf{x}-\mathbf{y})\,\delta_{il}$. Here $\delta(\cdot)$ is the Dirac delta function. Thus the Green's function is obtained as the solution to,

$$(\lambda+\mu)\frac{\partial^2}{\partial x_i\partial x_j}U^*_{jl}(\mathbf{x},\omega;\mathbf{y}) + \mu\frac{\partial^2}{\partial x_j\partial x_j}U^*_{il}(\mathbf{x},\omega;\mathbf{y}) + \delta(\mathbf{x}-\mathbf{y})\,\delta_{il} = -\rho\omega^2 U^*_{il}(\mathbf{x},\omega;\mathbf{y})\,. \tag{6}$$

The subscript l is not an index in the ordinary sense. It is used to indicate that there is not one, but *three* times three equations of motion, three for each $l = 1,2,3$. Subsequently, the subscript l will only be used to indicate the coordinate direction of the point load.

In order to find the displacement Green's function, the principle of Helmholz decomposition is used. This implies that each of the fields $B^*_{il}(\mathbf{x},\omega;\mathbf{y})$ and $U^*_{il}(\mathbf{x},\omega;\mathbf{y})$, defined on the domain Ω, may be written as the sum of the gradient to a scalar field and the rotation of a vector field, *i.e.*

$$B^*_{il}(\mathbf{x},\omega;\mathbf{y}) = \frac{\partial}{\partial x_i}\Phi_l(\mathbf{x},\omega;\mathbf{y}) + e_{ijk}\frac{\partial}{\partial x_j}\Psi_{kl}(\mathbf{x},\omega;\mathbf{y}), \tag{7}$$

$$U^*_{il}(\mathbf{x},\omega;\mathbf{y}) = \frac{\partial}{\partial x_i}\varphi_l(\mathbf{x},\omega;\mathbf{y}) + e_{ijk}\frac{\partial}{\partial x_j}\psi_{kl}(\mathbf{x},\omega;\mathbf{y}), \tag{8}$$

where e_{ijk} is the permutation symbol. The three scalar fields $\Phi_l(\mathbf{x},\omega;\mathbf{y})$ (one for each coordinate direction of the load, l) and the three vector fields $\Psi_{il}(\mathbf{x},\omega;\mathbf{y})$ are derived from the load field as

$$\Phi_l(\mathbf{x},\omega;\mathbf{y}) = -\frac{1}{4\pi}\frac{\partial}{\partial x_i}\int_\Omega \frac{1}{r}B^*_{il}(\mathbf{x},\omega;\mathbf{y})\,d\mathbf{y} = -\frac{1}{4\pi}\frac{\partial}{\partial x_l}\left(\frac{1}{r}\right), \tag{9}$$

$$\Psi_{il}(\mathbf{x},\omega;\mathbf{y}) = \frac{1}{4\pi}e_{ijk}\frac{\partial}{\partial x_j}\int_\Omega \frac{1}{r}B^*_{kl}(\mathbf{x},\omega;\mathbf{y})\,d\mathbf{y} = \frac{1}{4\pi}e_{ijl}\frac{\partial}{\partial x_j}\left(\frac{1}{r}\right). \tag{10}$$

Here $r = |\mathbf{x}-\mathbf{y}|$ is the distance between the *observation point* $\mathbf{x}$ and the *source point* $\mathbf{y}$. Taking the divergence and rotation, respectively, of Eq. (6) the following inhomogeneous frequency-domain wave equations are produced,

$$c_P^2\frac{\partial^2}{\partial x_j^2}\varphi_l(\mathbf{x},\omega;\mathbf{y}) - \frac{1}{4\pi\rho}\frac{\partial}{\partial x_l}\left(\frac{1}{r}\right) = -\omega^2\varphi_l(\mathbf{x},\omega;\mathbf{y}), \tag{11}$$

$$c_S^2\frac{\partial^2}{\partial x_j^2}\psi_{il}(\mathbf{x},\omega;\mathbf{y}) + \frac{1}{4\pi\rho}e_{ijl}\frac{\partial}{\partial x_j}\left(\frac{1}{r}\right) = -\omega^2\psi_{il}(\mathbf{x},\omega;\mathbf{y}). \tag{12}$$

where $c_P^2 = (\lambda+2\mu)/\rho$ and $c_S^2 = \mu/\rho$. These are identified as the phase velocities for *pressure* (or dilatational) and *shear* (or rotational) waves, respectively. It should be mentioned that the letters P and S origin from earthquake engineering and are acronyms for *primary* and *secondary* since the P-waves will arrive before the S-waves at any location not being the source point, given that $\lambda \geq 0$ which holds for all real materials. Next, the substitutions

$$\varphi_l(\mathbf{x},\omega;\mathbf{y}) = -\frac{\partial}{\partial x_l}p(\mathbf{x},\omega;\mathbf{y}), \quad \psi_{il}(\mathbf{x},\omega;\mathbf{y}) = e_{ijl}\frac{\partial}{\partial x_j}s(\mathbf{x},\omega;\mathbf{y}) \tag{13}$$

are introduced. Furthermore, let $k_P = \omega/c_P$ and $k_S = \omega/c_S$ denote the wave numbers for pressure and shear waves, respectively. Equations (11) and (12) may then be written,

$$\frac{\partial^2}{\partial x_j^2}p(\mathbf{x},\omega;\mathbf{y}) + \frac{1}{4\pi\rho c_P^2 r} = -k_P^2 p(\mathbf{x},\omega;\mathbf{y}), \quad \frac{\partial^2}{\partial x_j^2}s(\mathbf{x},\omega;\mathbf{y}) + \frac{1}{4\pi\rho c_S^2 r} = -k_S^2 s(\mathbf{x},\omega;\mathbf{y}). \tag{14}$$

The particular solutions to Equations (14) are both $p_p(\mathbf{x},\omega;\mathbf{y}) = s_p(\mathbf{x},\omega;\mathbf{y}) = -1/(4\pi\rho\omega^2 r)$, whereas the complimentary solutions are $p_c(\mathbf{x},\omega;\mathbf{y}) = c_1(1/r)e^{ik_P r} + c_2(1/r)e^{-ik_P r}$ and

$s_c(\mathbf{x},\omega;\mathbf{y}) = d_1\,(1/r)\,e^{ik_S r} + d_2\,(1/r)\,e^{-ik_S r}$. With the given definition of the harmonic time variation, *i.e.* a variation of type $e^{i\omega t}$, the first term of each of the complimentary solutions corresponds to waves coming in from infinity. For physical reasons these terms must be disregarded, *i.e.* $c_1 = d_1 = 0$, since energy must propagate away from the source. It should be noted that the group velocity $c_g = \partial\omega/\partial k$ in an infinite homogeneous elastic continuum, and therefore the velocity of energy propagation, is equal to the phase velocity $c = \omega/k$. When the Lamé constants are real, the phase velocities and therefore also the group velocities are independent of the frequency, *i.e.* the waves are not dispersive.

Subsequently, as the solution must be finite for $r \to 0$, the full solutions are derived as:

$$p(\mathbf{x},\omega;\mathbf{y}) = \frac{1}{4\pi\rho\omega^2 r}\left(e^{-ik_P r} - 1\right), \quad s(\mathbf{x},\omega;\mathbf{y}) = \frac{1}{4\pi\rho\omega^2 r}\left(e^{-ik_S r} - 1\right). \tag{15}$$

By differentiation of the solutions (15) as defined by Eq. (13) and subsequently Eqs. (7) and (8), the following Green's function is finally obtained for the amplitudes of the time harmonic displacements,

$$U^*_{il}(\mathbf{x},\omega;\mathbf{y}) = \frac{1}{4\pi\rho c_S^2}\left(\alpha\delta_{il} - \beta\frac{\partial r}{\partial x_i}\frac{\partial r}{\partial x_l}\right), \tag{16}$$

where

$$\alpha = \left(\frac{1}{r} + \frac{1}{ik_S r^2} - \frac{1}{k_S^2 r^3}\right)e^{-ik_S r} - \frac{c_S^2}{c_P^2}\left(\frac{1}{ik_P r^2} - \frac{1}{k_P^2 r^3}\right)e^{-ik_P r}, \tag{17}$$

$$\beta = \left(\frac{1}{r} + \frac{3}{ik_S r^2} - \frac{3}{k_S^2 r^3}\right)e^{-ik_S r} - \frac{c_S^2}{c_P^2}\left(\frac{1}{r} + \frac{3}{ik_P r^2} - \frac{3}{k_P^2 r^3}\right)e^{-ik_P r}. \tag{18}$$

2.2.2 Green's Function for the Stress Field

The frequency domain Green's function for the stress, $\Sigma^*_{ijl}(\mathbf{x},\omega;\mathbf{y})$, is derived by insertion of the displacement Green's function defined by Eqs. (16)-(18) into Eq. (2) formulated in the frequency domain, that is

$$\Sigma^*_{ijl}(\mathbf{x},\omega;\mathbf{y}) = \lambda\frac{\partial}{\partial x_k}U^*_{kl}(\mathbf{x},\omega;\mathbf{y})\,\delta_{ij} + \mu\left(\frac{\partial}{\partial x_i}U^*_{jl}(\mathbf{x},\omega;\mathbf{y}) + \frac{\partial}{\partial x_j}U^*_{il}(\mathbf{x},\omega;\mathbf{y})\right). \tag{19}$$

Expressed in terms of the parameters α and β, the stress Green's function reads

$$\begin{aligned}\Sigma^*_{ijl}(\mathbf{x},\omega;\mathbf{y}) = \frac{1}{4\pi}\Bigg[&\left(\frac{c_P^2}{c_S^2} - 2\right)\left(\frac{\partial\alpha}{\partial r} - \frac{\partial\beta}{\partial r} - \frac{2\beta}{r}\right)\frac{\partial r}{\partial x_l}\delta_{ij} + \frac{\partial\alpha}{\partial r}\left(\frac{\partial r}{\partial x_i}\delta_{jl} + \frac{\partial r}{\partial x_j}\delta_{il}\right) - \\ &\frac{\beta}{r}\left(\frac{\partial r}{\partial x_i}\delta_{jl} + \frac{\partial r}{\partial x_j}\delta_{il} + 2\frac{\partial r}{\partial x_l}\delta_{ij} - 4\frac{\partial r}{\partial x_i}\frac{\partial r}{\partial x_j}\frac{\partial r}{\partial x_l}\right) - 2\frac{\partial\beta}{\partial r}\frac{\partial r}{\partial x_i}\frac{\partial r}{\partial x_j}\frac{\partial r}{\partial x_l}\Bigg],\end{aligned} \tag{20}$$

where it has been used that $\lambda = \rho\,(c_P^2 - 2c_S^2)$ and $\mu = \rho c_S^2$. The directional derivatives $\partial\alpha/\partial r$ and $\partial\beta/\partial r$ are easily obtained from Eqs. (17) and (18),

$$\frac{\partial \alpha}{\partial r} = \left(-\frac{ik_S}{r} - \frac{2}{r^2} - \frac{3}{ik_S r^3} + \frac{3}{k_S^2 r^4} \right) e^{-ik_S r} + \frac{c_S^2}{c_P^2} \left(\frac{1}{r^2} + \frac{3}{ik_P r^3} - \frac{3}{k_P^2 r^4} \right) e^{-ik_P r}, \quad (21)$$

$$\frac{\partial \beta}{\partial r} = \left(-\frac{ik_S}{r} - \frac{4}{r^2} - \frac{9}{ik_S r^3} + \frac{9}{k_S^2 r^4} \right) e^{-ik_S r} + \frac{c_S^2}{c_P^2} \left(\frac{ik_P}{r} + \frac{4}{r^2} + \frac{9}{ik_P r^3} - \frac{9}{k_P^2 r^4} \right) e^{-ik_P r}. \quad (22)$$

2.2.3 Green's Function for the Surface Traction

The frequency domain Green's function for the surface traction, $P^*_{il}(\mathbf{x}, \omega; \mathbf{y})$, is obtained by taking the dot product between the stress Green's function tensor and the unit outward unit normal vector, n_i. This leads to the formulation

$$P^*_{il}(\mathbf{x}, \omega; \mathbf{y}) = \Sigma^*_{ijl}(\mathbf{x}, \omega; \mathbf{y})\, n_j \quad (23)$$

which after insertion of the result (20) gives

$$P^*_{il}(\mathbf{x}, \omega; \mathbf{y}) = \frac{1}{4\pi} \left[\left(\frac{c_P^2}{c_S^2} - 2 \right) \left(\frac{\partial \alpha}{\partial r} - \frac{\partial \beta}{\partial r} - \frac{2\beta}{r} \right) \frac{\partial r}{\partial x_l} n_i + \frac{\partial \alpha}{\partial r} \left(\frac{\partial r}{\partial x_i} n_l + \frac{\partial r}{\partial n} \delta_{il} \right) - \frac{\beta}{r} \left(\frac{\partial r}{\partial x_i} n_l + \frac{\partial r}{\partial n} \delta_{il} + 2 \frac{\partial r}{\partial x_l} n_i - 4 \frac{\partial r}{\partial x_i} \frac{\partial r}{\partial x_l} \frac{\partial r}{\partial n} \right) - 2 \frac{\partial \beta}{\partial r} \frac{\partial r}{\partial x_i} \frac{\partial r}{\partial x_l} \frac{\partial r}{\partial n} \right]. \quad (24)$$

Here $\partial r / \partial n$ is the derivative of the distance vector, $r_i = x_i - y_i$, in the direction of the outward unit normal vector .

2.3 Integral Formulation of the Elastodynamic Problem

Let two elastodynamic states be defined over the body Ω in the frequency domain. The two states have the complex amplitudes of displacement, traction and body forces $U_i^1(\mathbf{x}, \omega)$, $P_i^1(\mathbf{x}, \omega)$, $B_i^1(\mathbf{x}, \omega)$ and $U_i^2(\mathbf{x}, \omega)$, $P_i^2(\mathbf{x}, \omega)$, $B_i^2(\mathbf{x}, \omega)$, respectively. From the Betti Reciprocal Theorem the following relationship may be formulated between the two states [3],

$$\int_\Gamma P_i^1(\mathbf{x}, \omega)\, U_i^2(\mathbf{x}, \omega)\, d\Gamma + \int_\Omega \rho B_i^1(\mathbf{x}, \omega)\, U_i^2(\mathbf{x}, \omega)\, d\Omega = \int_\Gamma P_i^2(\mathbf{x}, \omega)\, U_i^1(\mathbf{x}, \omega)\, d\Gamma + \int_\Omega \rho B_i^2(\mathbf{x}, \omega)\, U_i^1(\mathbf{x}, \omega)\, d\Omega. \quad (25)$$

Taking $U_i^1(\mathbf{x}, \omega)$, $P_i^1(\mathbf{x}, \omega)$, $B_i^1(\mathbf{x}, \omega)$ as the state of real, physical displacements, tractions and body forces, and assuming that the second state corresponds to the fundamental solution, Equation (25) changes to

$$U_l(\mathbf{y}, \omega) + \int_\Gamma P^*_{il}(\mathbf{x}, \omega; \mathbf{y})\, U_i(\mathbf{x}, \omega)\, d\Gamma = \int_\Gamma U^*_{il}(\mathbf{x}, \omega; \mathbf{y})\, P_i(\mathbf{y}, \omega)\, d\Gamma + \int_\Omega \rho U^*_{il}(\mathbf{x}, \omega; \mathbf{y})\, B_i(\mathbf{x}, \omega)\, d\Omega. \quad (26)$$

Making use of the reciprocal relation $U^*_{il}(\mathbf{x},\omega;\mathbf{y}) = U^*_{li}(\mathbf{y},\omega;\mathbf{x})$ (which will not be proved here) and, furthermore, introducing the substitutions $i \rightarrow l$, $l \rightarrow i$ and $\mathbf{x} \rightarrow \mathbf{y}$, $\mathbf{y} \rightarrow \mathbf{x}$, Equation (26) is rewritten in the following form,

$$U_i(\mathbf{x},\omega) + \int_\Gamma P^*_{il}(\mathbf{x},\omega;\mathbf{y})\, U_l(\mathbf{y},\omega)\, d\Gamma = \int_\Gamma U^*_{il}(\mathbf{x},\omega;\mathbf{y})\, P_l(\mathbf{y},\omega)\, d\Gamma + \int_\Omega \rho U^*_{il}(\mathbf{x},\omega;\mathbf{y})\, B_l(\mathbf{y},\omega)\, d\Omega. \quad (27)$$

This equation holds for any observation point $\mathbf{x}$ which is interior to the domain Ω. In the absence of body forces, the integral equation for a point on the surface may be derived from Eq. (27), leading to the formulation

$$C_{il}(\mathbf{x})\, U_l(\mathbf{x},\omega) + \int_\Gamma P^*_{il}(\mathbf{x},\omega;\mathbf{y})\, U_l(\mathbf{y},\omega)\, d\Gamma = \int_\Gamma U^*_{il}(\mathbf{x},\omega;\mathbf{y})\, P_l(\mathbf{y},\omega)\, d\Gamma. \quad (28)$$

The tensor $C_{il}(\mathbf{x})$ depends solely on the geometry of the surface Γ at the point $\mathbf{y}$. $C_{il}(\mathbf{y}) = \frac{1}{2}\delta_{il}$ if the surface is smooth at $\mathbf{x}$. For any other configuration of the surface geometry at the observation point other values of $C_{il}(\mathbf{x})$ are obtained.

Equation (28) is referred to as Somigliana's Identity and forms the mathematical basis for the direct boundary integral and boundary element methods. It should be noted that the integrals over the Green's functions for both the displacement and traction are singular when the observation point $\mathbf{x}$ coincides with the source (or integration) point $\mathbf{y}$. These singular terms must be treated in a special way in the numerical integration as explained in Subsection 2.5, or the accuracy of the results will be reduced significantly.

2.4 Discretization Using Quadratic Shape Functions

The next step in the development of the BEM is to discretize the state variable fields $U_i(\mathbf{x},\omega)$ and $P_i(\mathbf{x},\omega)$ into the values at N so-called *collocation nodes*. Accordingly the surface intergral is exchanged with a sum of integrals over NE elements. The displacement and traction fields are interpolated over each element using a set of shape functions, which are also used to approximate the geometry, *i.e.* the elements are isoparametric. This step is similar to the finite element approach. However, the Green's functions are used as weight functions instead of the shape functions, which are used in a standard Galerkin FEM scheme. It should be noted that the BEM allows the use of *constant* elements, where the displacement and traction is assumed to be constant over the entire element leading to discontinuities at the element edges. This kind of element is however inadequate for most wave propagation problems as the convergence is very slow compared to that of higher order elements, *e.g.* quadratic elements which have been used in the present work. For flexural problems the constant elements do not work at all [3].

Let $\mathbf{U}_j(\omega)$ and $\mathbf{P}_j(\omega)$ be two $(3N_j \times 1)$ vectors storing the nodal displacements and tractions, respectively, for the N_j nodes in element j. Furthermore defining $\mathbf{x}_j$ as the $(3N_j \times 1)$

coordinate vector for the element nodes, the displacement and traction fields over the element surface Γ_j as well as the geometry may be described in vector form,

$$\mathbf{U}(\mathbf{x},\omega) = \mathbf{\Phi}_j(\mathbf{x})\,\mathbf{U}_j(\omega)\,, \quad \mathbf{P}(\mathbf{x},\omega) = \mathbf{\Phi}_j(\mathbf{x})\,\mathbf{P}_j(\omega)\,, \quad \mathbf{x} = \mathbf{\Phi}_j\mathbf{x}_j, \tag{29}$$

where $\mathbf{x}$ is a point (x_1, x_2, x_3) on the element surface Γ_j and $\mathbf{\Phi}_j(\mathbf{x})$ is a $(3 \times 3N_j)$ matrix storing the shape functions for the element,

$$\mathbf{\Phi}_j(\mathbf{x}) = \begin{bmatrix} \phi_1 & 0 & 0 & \phi_2 & 0 & 0 & \cdots & \phi_{N_j} & 0 & 0 \\ 0 & \phi_1 & 0 & 0 & \phi_2 & 0 & \cdots & 0 & \phi_{N_j} & 0 \\ 0 & 0 & \phi_1 & 0 & 0 & \phi_2 & \cdots & 0 & 0 & \phi_{N_j} \end{bmatrix}. \tag{30}$$

Each of the components ϕ_n, $n = 1, 2, \ldots, N_j$, is the shape function belonging to the nth element node and depends on the position $\mathbf{x}$ on the element surface. With the definitions in Equation (29) the discretized boundary intergral equation, *i.e.* the BEM formulation of Eq. (28), for a single collocation node with the coordinates $\mathbf{x}_i$ obtains the form

$$\mathbf{C}(\mathbf{x}_i)\,\mathbf{U}_i(\omega) + \sum_{j=1}^{NE} \left\{ \int_{\Gamma_j} \mathbf{P}^*(\mathbf{x}_i,\omega;\mathbf{y})\,\mathbf{\Phi}_j(\mathbf{y})\,d\Gamma_j \right\} \mathbf{U}_j(\omega) = \sum_{j=1}^{NE} \left\{ \int_{\Gamma_j} \mathbf{U}^*(\mathbf{x}_i,\omega;\mathbf{y})\,\mathbf{\Phi}_j(\mathbf{y})\,d\Gamma_j \right\} \mathbf{P}_j(\omega)\,, \tag{31}$$

where NE is the number of boundary elements in the domain and $\mathbf{U}_i(\omega)$ are the complex amplitudes of displacement at $\mathbf{x}_i$. Notice that the integrals over each of the element surfaces Γ_j is carried out with respect to the source point coordinates $\mathbf{y}$, not $\mathbf{x}_i$ which is a single point.

The N matrix equations for each of the collocation nodes in the BE domain may be assembled into a single, global matrix equation for the entire domain. In the present work an approach has been taken where neighbouring elements share the nodes along the common edge. As the displacement field must be continuous across the element boundaries, the contributions from all adjacent elements to an integration node may simply be added. However, the traction is not generally continuous across element edges. For example discontinuities arise at corners because the direction of the unit normal vector varies. This means that the contributions from adjacent elements to a collocation node have to be stored separately. With this in mind the global system of equations for the BE domain is given as

$$\underset{(3N \times 3N)}{\hat{\mathbf{C}}} + \underset{(3N \times 3N)}{\hat{\mathbf{H}}} \Big) \underset{(3N \times 1)}{\mathbf{U}} = \underset{(N' \times 3N)}{\hat{\mathbf{G}}} \underset{(3N \times 1)}{\mathbf{P}} \tag{32}$$

The $\hat{\mathbf{C}}$ matrix stores the (3×3) matrices $\mathbf{C}(\mathbf{x}_i)$ for each of the observation nodes along the diagonal and is otherwise empty. The values of the integrals over the Green's functions for the traction and displacement are stored in $\hat{\mathbf{H}}$ and $\hat{\mathbf{G}}$, respectively, and $\mathbf{U}$ and $\mathbf{P}$ are vectors with the displacements and tractions at each node and for each degree of freedom. Underneath the

equation the dimension of each matrix/vector is given. For the $\hat{\mathbf{G}}$ matrix, $N' = 3\sum_{j=1}^{NE} N_j$ is the sum of degrees of freedom in each of the elements, keeping the degrees of freedom for multiple coincident element nodes separately.

In the computer program BEASTS that has been developed in the present project, the BE system of equations is eventually transformed into a finite element one, see Section 3. This means that discontinuous tractions are not allowed in the model, which may suggest that the model is not accurate when discontinuous tractions are actually present in the problem being analysed. It is therefore checked by numerical experiment that no significant discrepancies arise in the results obtained with such a model compared to the results calculated with the original BE model, see Section 4. When the FE approach is used, the tractions are continuous in the same way as the displacements. Hence a reduced version of the original matrix $\hat{\mathbf{G}}$ may be used. In the new matrix $\mathbf{G}$ the contributions to a collocation node from different elements are added. Furthermore, introducing $\mathbf{H} = \hat{\mathbf{C}} + \hat{\mathbf{H}}$, Equation (32) reduces to

$$\underset{(3N\times 3N)}{\mathbf{H}} \quad \underset{(3N\times 1)}{\mathbf{U}} \quad = \quad \underset{(3N\times 3N)}{\mathbf{G}} \quad \underset{(3N\times 1)}{\mathbf{P}} \tag{33}$$

which is the matrix equation established for each of the domains in the program BEASTS.

For any combination of collocation nodes and integration nodes that are not coincident, *i.e.* $\mathbf{x}_i \neq \mathbf{y}_i$, a standard Gauss-Legendre quadrature rule may be used for numerical integration over each element, given that the element geometry is described in terms of homogeneous coordinates, as discussed below. However, when the collocation node is the same as the integration node, singularities arise in the integrals over the Green's functions. A means of dealing with these singular terms is developed in Subsection 2.5.

In the computer program BEASTS there are two types of boundary elements available: a nine-noded quadrilateral element with biquadratic interpolation and a six-noded triangular element with quadratic interpolation. As the direction of the normal vector $\mathbf{n}$ is essential to the calculation of the traction terms, the direction of the normal vector must be determined uniquely from the element topology. This is ensured by always numbering the nodes in clockwise order around the element when looking in the direction of the normal vector, *i.e.* out from the domain. The node ordering is illustrated on Figure 2.

In order to use a standard Gauss-Legendre quadrature rule for the numerical integration, each of the curved elements must first be mapped into a generic element. Hence, a local (ξ_1, ξ_2) coordinate system is established for the quadrilateral elements, see Figure 2 (a). The elements are mapped into this plane coordinate system so that any point on the part of the boundary that belongs to the element lies within the square defined by $-1 \leq \xi_1 \leq 1$ and $-1 \leq \xi_2 \leq 1$. Expressed in terms of ξ_1 and ξ_2 the nine biquadratic shape functions ϕ_n, $n = 1, 2, \ldots, 9$, for the quadrilateral element may be written as

$$\begin{aligned}
&\phi_1 = \tfrac{1}{4}(\xi_1^2 - \xi_1)(\xi_2^2 - \xi_2), \quad \phi_2 = \tfrac{1}{2}(1 - \xi_1^2)(\xi_2^2 - \xi_2), \quad \phi_3 = \tfrac{1}{4}(\xi_1 + \xi_1^2)(\xi_2^2 - \xi_2), \\
&\phi_4 = \tfrac{1}{2}(\xi_1 + \xi_1^2)(1 - \xi_2^2), \quad \phi_5 = \tfrac{1}{4}(\xi_1 + \xi_1^2)(\xi_2 + \xi_2^2), \quad \phi_6 = \tfrac{1}{2}(1 - \xi_1^2)(\xi_2 + \xi_2^2), \\
&\phi_7 = \tfrac{1}{4}(\xi_1^2 - \xi_1)(\xi_2 + \xi_2^2), \quad \phi_8 = \tfrac{1}{2}(\xi_1^2 - \xi_1)(1 - \xi_2^2), \quad \phi_9 = (1 - \xi_1^2)(1 - \xi_2^2).
\end{aligned} \tag{34}$$

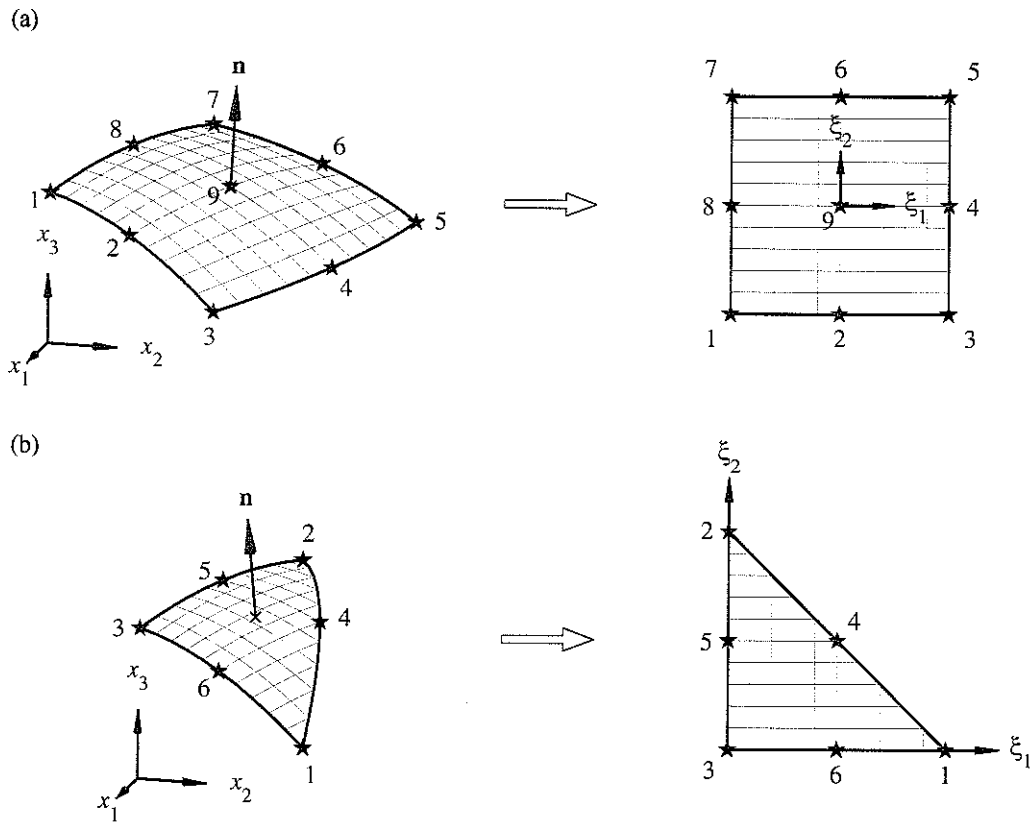

Figure 2. Mapping from 3D Cartesian coordinate space (x_1, x_2, x_3) into plane local coordinates (ξ_1, ξ_2): (a) Nine-noded quadrilateral element with biquadratic interpolation, (b) six-noded triangular element with quadratic interpolation. The normal vectors **n** are pointing out from the domain.

Similarly for the triangular elements the six quadratic shape functions are defined for a local plane coordinate system as illustrated on Figure 2 (b). The $N_j = 6$ shape functions are:

$$\begin{aligned} &\phi_1 = \xi_1(2\xi_1 - 1), \quad \phi_2 = \xi_2(2\xi_2 - 1), \quad \phi_3 = \xi_3(2\xi_3 - 1), \\ &\phi_4 = 4\xi_1\xi_2, \qquad \phi_5 = 4\xi_2\xi_3, \qquad \phi_6 = 4\xi_3\xi_1, \end{aligned} \tag{35}$$

where $0 \leq \xi_1 \leq 1$ and $0 \leq \xi_2 \leq 1 - \xi_1$. The third local coordinate $\xi_3 = 1 - \xi_1 - \xi_2$ is dependent on the first two coordinates and has been introduced for convenience only.

When the integration is performed over a single element in the local, homogeneous coordinate system, the area as well as the shape of the element, is misinterpreted. A transformation of the surface differential from the local plane coordinates to the three-dimensional Cartesian coordinate space is given by

$$d\Gamma = |\mathbf{J}(\xi_1, \xi_2)| \, d\xi_1 d\xi_2. \tag{36}$$

where $|\mathbf{J}(\xi_1, \xi_2)|$ is the magnitude of the Jacobian which is actually just the length of the normal vector (*not* the unit normal vector **n**) at the point.

2.5 Evaluation of Singular Terms for an Open Domain

For the main part of the numerical integration, a six-point Gauss-Legendre quadrature rule is used. In the finite element method where the quadratic shape functions would also be used as the weighting functions, a two-point rule would be sufficient. However the BEM used the Green's function as weighting functions. For the three-dimensional problem these are exponential functions, meaning that a higher order of accuracy in the discretization will always be gained by using more Gauss points per element.

When the collocation node is one of the nodes in the element over which the integration is carried out, the standard integration is not satisfactory, as singularities arise in the Green's functions for the displacement and the traction. The next subsection explains how the different singularities are handled in the program BEASTS.

2.5.1 Singularities of the Displacement Green's Function

The terms of the matrix $\mathbf{G}$ contain singularities of the the type $1/r$ when the collocation node coincides with the integration node. This is seen by considering Eq. (16) and substituting the exponential terms in Eqs. (17) to (18) by their Taylor series expansions, $e^{-ikr} = \sum_{n=0}^{\infty} \frac{1}{n!}(ikr)^n$. To carry out the numerical integration using a standard Gauss-Legendre quadrature over an element where the collocation node is one of the element nodes, Dominguez [3] used a method proposed by Lachat [8]. The main steps in the procedure are:

1. The element is divided into a number of triangles, each having one of the corners at the collocation node (see Figure 3).

2. The integral over each of the triangles is performed using a standard Gauss-Legendre quadrature rule over an equivalent *collapsed quadratic element*, but only for the shape function belonging to the element node which is also the collocation node. The technique is further explained below.

3. For all other shape functions a integration is carried out in the same way that is used for elements where the collocation node is not one of the element nodes.

The collapsed quadrilateral elements are quadrilateral elements where two of the corner nodes coincide so that one of the element sides has a length of zero, see Figure 4. When performing the numerical integration over an element with such a geometry, the Jacobian will tend to zero with r as $r \to 0$. This zero of the type r cancels out the $1/r$ singularity. Hence the accuracy of the Gauss-Legendre quadrature is satisfactory.

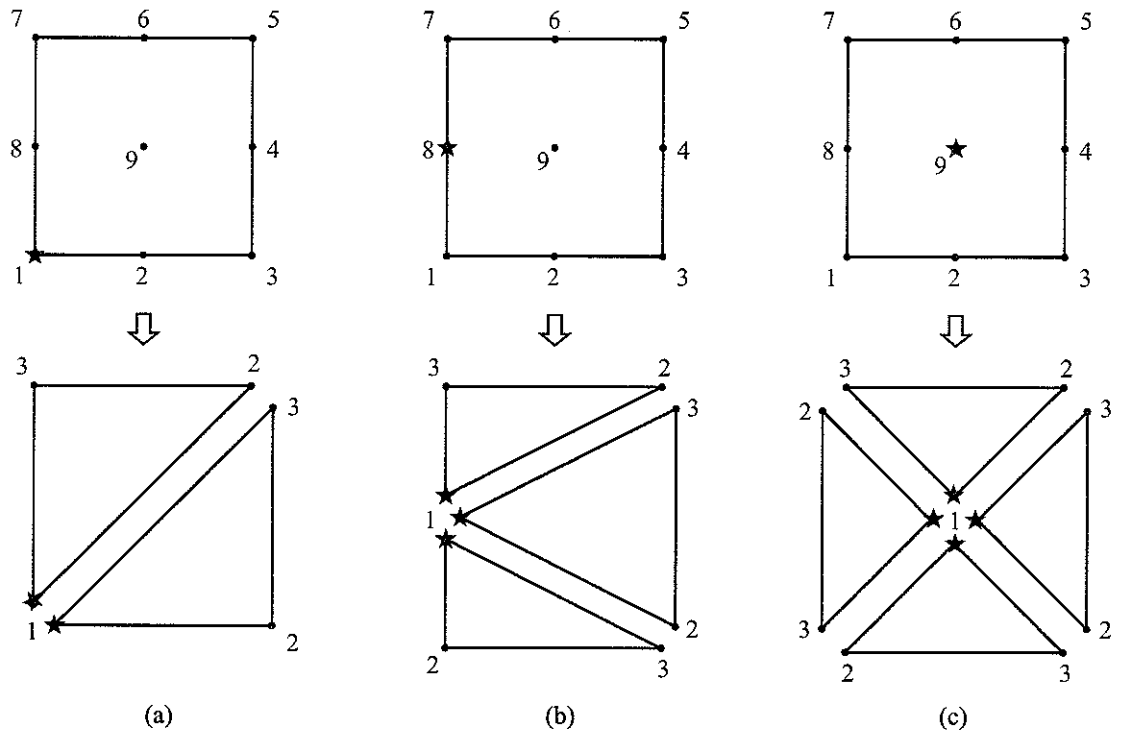

Figure 3. Sub-division of a quadrilateral element when (a) the collocation node is at a corner, (b) the collocation node is at a side and (c) the collocation node is at the centre of the element.

2.5.2 Singularities of the Traction Green's Function

The singularities of the traction Green's function and thus the singularities of the matrix $\mathbf{H}$ are of the kind $1/r^2$ when the observation point coincides with the integration point. Therefore the method proposed by Lachat does not provide a means of dealing with the diagonal terms of the matrix $\mathbf{H}$. To treat singularities of higher order than $1/r$ an alternative method has to be used. In the present work a numerical method is proposed. It is based on static equilibrium considerations for the surface tractions which normally only apply to closed domains [3]. To generalise the method to cover open domains where parts of the boundary are not discretized, a modified version of the *enclosing elements* technique proposed by Ahmad and Banerjee [1] is developed.

The basis for the numerical method proposed by Dominguez and others for closed domains is that the singularity in the dynamic frequency domain solution is the same as that of the static solution. Hence, writing the total dynamic Green's function matrix $\hat{\mathbf{H}}$ for the stress as the sum of the static part $\hat{\mathbf{H}}_S$ and the dynamic residue matrix $\mathbf{H}_R$,

$$\hat{\mathbf{H}} = \hat{\mathbf{H}}_S + \mathbf{H}_R, \tag{37}$$

only the singularities of the static part $\hat{\mathbf{H}}_S$ need to be treated in a special way. The remainder $\mathbf{H}_R$ may be determined using a standard Gauss-Legendre quadrature, since it contains no singularities. In the three-dimensional case the rest term is derived by writing the exponential terms

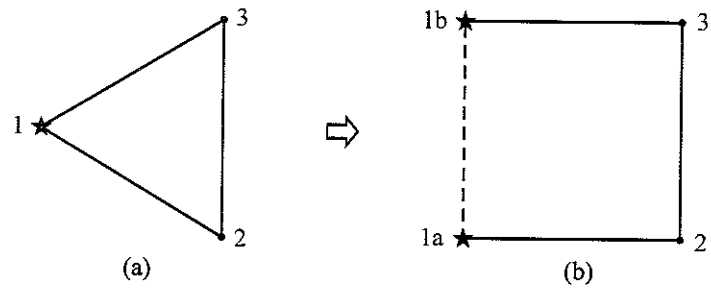

Figure 4. Sub-element for integraton of $1/r$ sigularities: (a) triangular sub-element and (b) equivalent collapsed quadrilateral element.

of the full elastodynamic solution as series expansions and subtracting the terms corresponding to the elastostatic Green's function [3].

The three-dimensional elastostatic traction Green's function is the special case of the elastodynamic fundamental solution given by Equation (24) that is obtained for the frequency $\omega = 0$. After rearranging the terms, the following solution is obtained:

$$P^*_{Sil}(\mathbf{x},\omega;\mathbf{y}) = -\frac{1}{8\pi\,(1-\nu)}\frac{1}{r^2}\left\{\frac{\partial r}{\partial n}\left((1-2\nu)\,\delta_{il}+3\frac{\partial r}{\partial x_i}\frac{\partial r}{\partial x_l}\right)+ (1-2\nu)\left(n_i\frac{\partial r}{\partial x_l}-n_l\frac{\partial r}{\partial x_i}\right)\right\}. \quad (38)$$

Here $P^*_{Sil}(\mathbf{x},\omega;\mathbf{y})$ is expressed in terms of the Poisson ratio ν, which is related to the Lamé constants as $\nu = \lambda/\left(2(\lambda+\mu)\right)$. The $1/r^2$ singularity is obvious in the static Green's function. As the static part $\hat{\mathbf{H}}_S$ is constant, regardless of the frequency, it may be evaluated once and for all and added to the dynamic rest term $\mathbf{H}_R$, which is calculated for each individual frequency.

In principle, the singular terms of $P^*_{Sil}(\mathbf{x},\omega;\mathbf{y})$ may be calculated analytically for any given geometry. For a smooth/flat part of the surface, the singular terms at the coinciding observation and source point cancel out because the normal vector $\mathbf{n}$ is perpendicular to the distance vector $\mathbf{r}$. Thus, the displacement should only be multiplied by the geometrical constant 0.5. However for arbitrary geometries, *e.g.* at a corner, the singular terms are not zero and the geometrical constant is different from 0.5. As the geometry may be quite complicated when quadratic interpolation is used, an integration by analytical means becomes complicated. Therefore a numerical method for dealing with the singularities as well as the geometry constants is preferred.

Dominguez [3] proposed a numerical method whereby the total contribution from the singular terms for $P^*_{Sil}(\mathbf{x},\omega;\mathbf{y})$ and the geometry constants may be derived. For a closed, interior domain with no tractions applied on any part of the surface, there should be no local deformations. Only a rigid body motion is possible, implying that all N (3×1) nodal displacement vectors in the BE model of the domain are the same. Combining this with the matrix equation, Eq. (33), for the entire system leads to the N sub-matrix equations (one for each node i):

$$\left(\mathbf{C}(\mathbf{x}_i)+\sum_{j=1}^{N}\hat{\mathbf{H}}_{Sij}\right)\mathbf{U_0}=\mathbf{0}, \quad (39)$$

where $\mathbf{U_0}$ is the arbitrary rigid body motion, which is generally different from $\mathbf{0}$, and $\hat{\mathbf{H}}_{Sij}$ are (3×3) sub-matrices of $\mathbf{H}_S$. Hence, the diagonal terms (or in fact the 3 by 3 sub-matrices along the diagonal) of the matrix $\mathbf{H}_S$ (including both $\hat{\mathbf{H}}_S$ and $\hat{\mathbf{C}}$) may be evaluated as

$$\mathbf{H}_{Sii} = \mathbf{C}(\mathbf{x}_i) + \hat{\mathbf{H}}_{Sii} = -\sum_{j=1, j\neq i}^{N} \hat{\mathbf{H}}_{Sij}. \tag{40}$$

For an open domain the method described above obviously makes no sense as parts of the boundary are not described in the model. To overcome this problem Ahmad and Banerjee [1] proposed that an artificial, enclosing boundary is constructed, merely for the evaluation of the singular diagonal terms of $\mathbf{H}_S$ and the geometry constants. This is plausible because the geometry constants only depend on the local geometry of the surface. This also applies to the singularities of $\hat{\mathbf{H}}_S$ since they arise in the contributions from a node to itself. Hence, any *closed* region which has the correct local geometry for the true surface may be used instead of the original *open* region for the purpose of determining $\mathbf{H}_{Sii}$. Any shape of the domain will do for the evaluation of the diagonal terms of $\hat{\mathbf{H}}_S$ given that the following requirements are met:

1. The distance between original elements and new, opposing elements must be at least one element length to ensure sufficient precision. Otherwise singularities may arise in the contributions from new nodes to existing nodes and vice versa.

2. The original geometry is modelled correctly at the nodes, for which the $\mathbf{H}_{Sii}$ terms are to be found. In principle this only requires that the elements adjacent to the node in question are taken from the original model.

The first point is a general rule of thumb for BE discretization and hence does not impose any restrictions that are not already there. From the second point, it may be concluded that it is not necessary to model the entire original open region and then add a number of extra elements to establish a single, global closed domain. Instead the terms for each node may be evaluated by creating a small closed domain around that specific node. This method of *local enclosing elements*, which was first proposed by Jones and Thompson [5] for the two dimensional case, has the following advantages compared to the original enclosing elements technique:

- It may be faster/more efficient to find the solution to numerous small systems of equations than to a single big system of equations.

- A local geometry for enclosing elements may easily be established automatically whereas the construction of an enclosing boundary for the entire domain may require an extensive amount of error checking to ensure that the enclosing elements do not intersect the true surface.

- The method may be applied to closed domains as well as open domains. This simplifies the programming of a general routine to find the $\mathbf{H}_{Sii}$ terms.

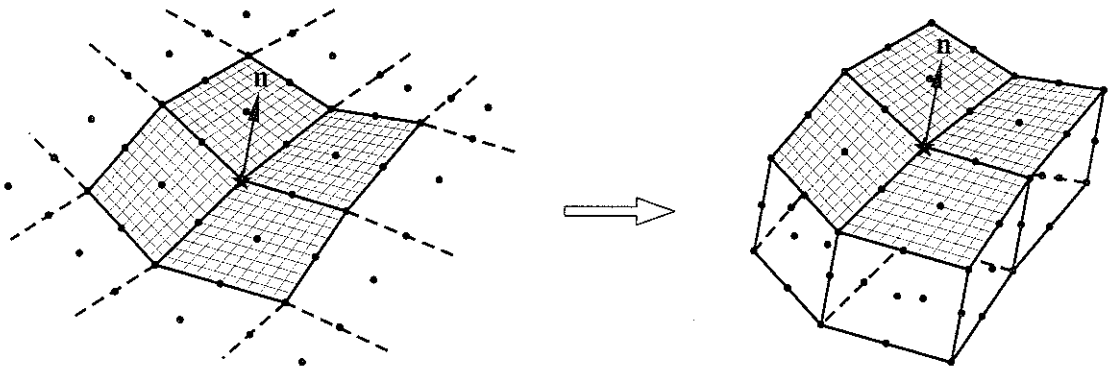

Figure 5. Construction of a false surface for a closed local domain: (a) a corner node on the original surface is picked and (b) the local domain is formed.

Several ways to pick out a local part of the entire surface may be suggested. The method implemented in the program BEASTS [2] has the following steps:

1. A loop is performed over all nodes, $i = 1, \ldots, N$, disregarding nodes that are not at the corner of an element.
2. The NE_i elements in the original model to which the selected corner node i belongs are identified.
3. A copy of the original elements adjacent to the corner node is offset a distance of approximately one element length in the direction of the inward normal (that is $-\mathbf{n}$).
4. The gap between the original surface elements and the copy is filled with NE_i elements, thereby producing a closed domain.
5. $\mathbf{H}_{Sii}$ is calculated using Eq. (40) for the corner node i and the neighbouring mid-side or centre nodes. These nodes are all on a part of the surface where the geometry is unchanged from the original open domain and will thus be determined correctly.

The method has been illustrated in Figure 5 and the five points in the procedure will be explained in the following.

Ad. 1. Generally corner nodes are identified as nodes that belong to three or more elements. A centre node of a nine-noded quadrilateral element belongs to only one element, and a mid-side node of either a six-noded triangular element or a nine-noded quadrilateral element belongs to two elements. Only at the edge, *i.e.* where the model of the open domain ends, does special care have to be shown.

Ad. 2. When identifying the elements to which the selected node belongs, it should be checked if the node is not a corner node in one/some of the elements. Definitely the node should

not be the centre-node of a quadrilateral element, but also it is bad discretization practice to join side-nodes with corner nodes. This would mean that the displacements along the element junctions are inconsistent as the shape functions for corner and side-nodes are not the same.

Ad. 3. By copying the original elements in the direction of the inward normal vector it is assured that the local closed domain is on the correct side of the true surface. When the surface is not flat at the selected corner node, the normal vector at the node is different for each element. To ensure that the projection vector points away from all adjacent elements and into the domain, the projection vector may be taken as a weighted average of the inward normal vectors.

Ad. 4. The distance between the two parts of the local surface consisting of the original NE_i elements and the copy thereof need only be of the same order as the distance across these two surfaces. Hence, one element in the $-\mathbf{n}$ direction should be sufficient to fill in the gap. By experiment it has been shown that adding another 'layer' of elements will not improve the accuracy significantly, whereas the calculation time is increased significantly.

Ad. 5. $\mathbf{H}_{Sii}$ is determined twice for mid-side nodes, and for centre nodes $\mathbf{H}_{Sii}$ may be determined multiple times. To reduce computation time it is advantageous to keep track of nodes which have already been analysed. However, the method described ensures that $\mathbf{H}_{Sii}$ is determined for each node at least once.

For some geometries of the surface in the model of the original open domain, the method described above may lead to significant errors in the determination of $\mathbf{H}_{Sii}$ and thus in the solution to the entire problem. Generally, to get an accurate solution the following conditions should apply:

- all sides of an element should have lengths of the same order of magnitude,
- contiguous elements must be of similar size,
- the angle between two elements should not be close to 2π,
- only slightly curved elements should be used.

In any case these conditions represent good practice for BE analysis of wave propagation problem. Hence, the fact that the method will only produce accurate results under these circumstances should not cause a difficulty in practice.

As an alternative to the described method, a bigger part of the boundary (*i.e.* more elements) may be picked out at a time, meaning that the local closed domain would consist of more elements and that the $\mathbf{H}_{Sii}$ terms would be determined for more nodes simultaneously. However, this would complicate the construction of the false surface since a general means of establishing the projection vector cannot be found. Moreover the described method has been tested for several different geometries and has been found to work satisfactorily.

2.6 Division of a Model into Sub-Domains

In the previous subsections, a formulation has been given for a single boundary element domain, which may be open or closed. The use of such a model is however restricted to the analysis of a loaded homogeneous half-space with arbitrary surface geometry or to a structure built from a single homogeneous material. A model which may be used for the analysis of a layered ground with an arbitrary geometry of the ground surface and the layer interfaces may be constructed by coupling a number of boundary element domains. The system matrices $\mathbf{G}_{ibed}$ and $\mathbf{H}_{ibed}$ for each of the $ibed = 1, 2, \ldots, nbed$ boundary element domains are constructed as described in Subsections 2.2 to 2.5.

Further domains may be used to describe built structures located beneath or on top of the ground surface, *e.g.* a tunnel or a railway track, given that the structures can be divided into a number of homogeneous regions. However, to obtain accurate results with the boundary element method, elements that do not belong to the same part of a surface or interface must not be close. Generally, distances less than one element length between two surfaces should be avoided. Otherwise the singularities of the Green's functions will lead to errors if a standard quadrature rule is used for numerical integration [5].

Hence, boundary elements are not suited for the modelling of thin structures or structures with detailed geometries. Here a finite element model is appropriate. For instance shell finite elements may be used to model a tunnel lining more efficiently than boundary elements, and in a local region with soil parameters shifting rapidly within short distances, solid finite elements may be used.

Thus, a model where both boundary and finite elements are available is useful for the analysis of problems involving a combination of (semi) infinite regions (*e.g.* a layered ground) and built structures (*e.g.* a tunnel). In Section 3 it is described how such a model may be constructed. Also the choice of coupling method for implementation in the BEASTS software [2] is discussed.

3 Coupling of Multiple Boundary Element Domains

This section describes how multiple boundary element domains may be coupled to form a global system of equations representing the entire model for a given frequency. The coupling is established on the basis of continuity of the displacement and equilibrium of the forces at the interfaces. For future use it is worthwhile to perform the coupling in a way that allows for a simple implementation of finite elements in addition to the boundary elements. The main problem in performing the coupling of a boundary element domain and finite element domain is that the forces at the interface in the boundary element method are described in terms of *tractions* distributed over the element surface, whereas a description in terms of *nodal forces* is used in the finite element method. This leads to two approaches to the coupling of BE and FE matrices. In both it is assumed that the nodes of the neighbouring BE and/or FE sub-domains coincide.

1. The coupling may be carried out in the finite element sense by transforming each of the boundary element domains to a *macro finite element*. An equivalent dynamic finite element stiffness matrix is derived from the BE system matrices $\mathbf{G}_{ibed}$ and $\mathbf{H}_{ibed}$, and the surface tractions are transformed into nodal forces.

2. The coupling may be carried out on the basis of equilibrium of the tractions on the interfaces. For this, the FE dynamic stiffness matrix must be transformed to one in terms of tractions on the boundary.

The first of these options has been implemented in the software developed in the present project, even if the computer program BEASTS does not facilitate any finite elements at the present stage. This allows the resulting dynamic stiffness matrices for the individual BE domains to be coupled in the finite element sense and for the response of the whole model to applied nodal forces to be calculated. The method is described in Subsection 3.1. The second approach has computational advantages but does not provide a simple means of dealing with the problem of coupling at points where the implied tractions are discontinuous. Although it has not been applied in the present work the method is described in Subsection 3.2 for future use. In Subsection 3.3 a further discussion on why the FE approach has been chosen may be found.

3.1 Coupling in a Finite Element Sense

In the time domain, the work done by the surface tractions $\mathbf{p}(\mathbf{x},t)$ at a part Γ_p of the boundary in applying a virtual displacement field $\delta\mathbf{u}(\mathbf{x},t)$ is given as

$$\delta w = \int_{\Gamma_p} \{\delta\mathbf{u}(\mathbf{x},t)\}^T \mathbf{p}(\mathbf{x},t)\, d\Gamma. \tag{41}$$

The vectors describing the traction and virtual displacement fields are column vectors with the three components $p_j(\mathbf{x},t)$ and $u_j(\mathbf{x},t)$, $j = 1,2,3$, respectively.

Consider a single finite, or boundary, element on which tractions are applied at the boundary $\Gamma_j \in \Gamma_p$. The nodal displacements and tractions may be stacked in two column vectors $\mathbf{u}_j(t)$ and $\mathbf{p}_j(t)$, which will have $3 \times N_j$ rows in the three-dimensional case. Using the element shape functions to interpolate the displacements and the tractions, the field quantities at any point on the element surface become $\mathbf{u}(\mathbf{x},t) = \mathbf{\Phi}_j(\mathbf{x})\,\mathbf{u}_j(t)$ and $\mathbf{p}(\mathbf{x},t) = \mathbf{\Phi}_j(\mathbf{x})\,\mathbf{p}_j(t)$, respectively. Thus the work done for element j may be written

$$\delta w_j = \{\delta\mathbf{u}_j(t)\} \int_{\Gamma_j} \{\mathbf{\Phi}_j(\mathbf{x})\}^T \mathbf{\Phi}_j(\mathbf{x})\, d\Gamma\, \mathbf{p}_j(t)\,. \tag{42}$$

The work done by the surface tractions is equal to the work done by the equivalent nodal forces $\mathbf{f}_j(t)$ that would imply the same virtual displacement values, $\delta\mathbf{u}_j(t)$, at the nodes, that is,

$$\delta w_j = \{\delta\mathbf{u}_j(t)\}\,\mathbf{f}_j(t)\,. \tag{43}$$

Combining Eqs. (42) and (43), the following relationship is derived,

$$\mathbf{f}_j(t) = \int_{\Gamma_j} \{\mathbf{\Phi}_j(\mathbf{x})\}^T \mathbf{\Phi}_j(\mathbf{x})\, d\Gamma\, \mathbf{p}_j(t)\,. \tag{44}$$

This provides a matrix expression where the shape functions are used to transform the surface tractions $\mathbf{p}_j(t)$ on element j into the equivalent nodal forces $\mathbf{f}_j(t)$. In the frequency domain the transformation process becomes

$$\mathbf{F}_j(\omega) = \int_{\Gamma_j} \{\mathbf{\Phi}_j(\mathbf{x})\}^T \mathbf{\Phi}_j(\mathbf{x})\, d\Gamma\, \mathbf{P}_j(\omega)\,, \tag{45}$$

where $\mathbf{F}_j(\omega)$ and $\mathbf{P}_j(\omega)$ are the complex amplitudes of the nodal forces and tranctions, respectively.

Calculating the element transformation matrices represented by the integral in Eq. (45) for all elements $j = 1, 2, \ldots, J$ in BE domain *ibed* and assembling them into a global system for the domain yields a transformation matrix $\mathbf{T}_{ibed}$ such that

$$\mathbf{F}_{ibed} = \mathbf{T}_{ibed}\mathbf{P}_{ibed}. \tag{46}$$

Here $\mathbf{F}_{ibed}$ is a vector of nodal forces equivalent to the nodal tractions $\mathbf{P}_{ibed}$ applied on the domain. The dimension of the system (*i.e.* the number of rows in $\mathbf{F}_{ibed}$, $\mathbf{T}_{ibed}$ and $\mathbf{P}_{ibed}$ as well as the number of columns in $\mathbf{T}_{ibed}$) is equal to the number of degrees of freedom in the domain. For a three-dimensional, elastodynamic BE domain that is three times the number of nodes in the domain. The transformation matrix $\mathbf{T}_{ibed}$ is sparse. Due to the nature of the element shape function matrices $\mathbf{\Phi}_j$ two out of three components are in all cases equal to zero, and furthermore only parts of the matrix $\mathbf{T}_{ibed}$ that belong to nodes of the same element will be filled.

Now consider the boundary element equation for a single domain, *i.e.* Equation (33) with subscript *ibed* on each of the matrices and vectors. Premultiplication by $\mathbf{T}_{ibed}\{\mathbf{G}_{ibed}\}^{-1}$ leads to the formulation

$$\left[\mathbf{T}_{ibed}\{\mathbf{G}_{ibed}\}^{-1}\mathbf{H}_{ibed}\right]\mathbf{U}_{ibed} = \mathbf{T}_{ibed}\mathbf{P}_{ibed} = \mathbf{F}_{ibed}. \tag{47}$$

This defines $\left[\mathbf{T}_{ibed}\{\mathbf{G}_{ibed}\}^{-1}\mathbf{H}_{ibed}\right] = \mathbf{K}_{ibed}$ as the dynamic stiffness matrix for boundary element domain *ibed*. The matrix $\mathbf{K}_{ibed}$ relates the nodal displacements to the nodal forces applied to the domain instead of the nodal tractions, as is the case in the original BE formulation. For a number of BE domains the $ibed = 1, 2, \ldots, nbed$ stiffness matrices $\mathbf{K}_{ibed}$ may therefore be assembled in the FE sense along with any finite elements into a global stiffness matrix $\mathbf{K}$ representing the entire model.

As already mentioned, the present transformation method turns each boundary element domain into a kind of macro finite element, that is a finite element with as many nodes as are used in the BE domain. Since the Green's functions are used as weighting functions, all degrees of freedom in the individual BE domains are coupled, meaning that the matrices $\mathbf{K}_{ibed}$ are full. However, the global system matrix $\mathbf{K}$ will only have a limited bandwidth, as is common for FE matrices, given that only some of the nodes are coupled at the interface.

Another thing worth mentioning is that the BE stiffness matrices produced in this way do not have the usual FE property of symmetry, which is a disadvantage with respect to memory storage space. Mustoe [9] suggested a method by which a symmetric boundary element stiffness matrix can be produced. The method is however slightly more complicated than the method presented in this section, and furthermore the inversion of a matrix twice the size of $\mathbf{K}_{ibed}$ has to be carried out. This is a major disadvantage as inverting the $\mathbf{G}_{ibed}$ matrix is already a time consuming process.

Tullberg and Bolteus [11] conducted a study of seven different stiffness matrices for a BE domain, including the original non-symmetric stiffness matrix and six symmetric matrices. The main conclusions from their study is:

1. The direct non-symmetric stiffness matrix, *i.e.* the matrix derived above, is the best in terms of accuracy.
2. The direct non-symmetric stiffness matrix is as good as, or better than, a stiffness matrix based on a finite element discretization with the same number of degrees of freedom. The same conclusion was drawn by Jones *et al.* [7].
3. The manipulated methods involving symmetric matrices show a very poor rate of convergence compared to the direct BE.

For these reasons it has been chosen to implement the non-symmetric stiffness matrix, the derivation of which has been given in this section, in the software described in [2].

3.2 Coupling in a Boundary Element Sense

Instead of transforming the BE system matrices to an equivalent FE stiffness matrix and performing the coupling in a finite element sense, the boundary element method formulation may be used. This means that equilibrium of the tractions has to be ensured on the interface, rather than equilibrium of nodal forces. For a coupling with finite elements, this implies that a reformulation of the FE system matrices has to be carried out, but even for a pure BE model problems arise in this method as will be described in the next subsection.

First, consider a single boundary element domain, *ibed*. Reordering the rows and columns into components belonging to the interface (superscript I) and the rest of the domain (superscript R) the matrix equation (33) takes the form

$$\begin{bmatrix} \mathbf{H}_{ibed}^{RR} & \mathbf{H}_{ibed}^{RI} \\ \mathbf{H}_{ibed}^{IR} & \mathbf{H}_{ibed}^{II} \end{bmatrix} \begin{bmatrix} \mathbf{U}_{ibed}^{R} \\ \mathbf{U}_{ibed}^{I} \end{bmatrix} = \begin{bmatrix} \mathbf{G}_{ibed}^{RR} & \mathbf{G}_{ibed}^{RI} \\ \mathbf{G}_{ibed}^{IR} & \mathbf{G}_{ibed}^{II} \end{bmatrix} \begin{bmatrix} \mathbf{P}_{ibed}^{R} \\ \mathbf{P}_{ibed}^{I} \end{bmatrix}. \tag{48}$$

Next, for a finite element domain, similarly the system of equations becomes

$$\begin{bmatrix} \mathbf{K}_{FE}^{RR} & \mathbf{K}_{FE}^{RI} \\ \mathbf{K}_{FE}^{IR} & \mathbf{K}_{FE}^{II} \end{bmatrix} \begin{bmatrix} \mathbf{U}_{FE}^{R} \\ \mathbf{U}_{FE}^{I} \end{bmatrix} = \begin{bmatrix} \mathbf{F}_{FE}^{R} \\ \mathbf{F}_{FE}^{I} \end{bmatrix} = \begin{bmatrix} \mathbf{T}_{FE}^{RR} & \mathbf{T}_{FE}^{RI} \\ \mathbf{T}_{FE}^{IR} & \mathbf{T}_{FE}^{II} \end{bmatrix} \begin{bmatrix} \mathbf{P}_{FE}^{R} \\ \mathbf{P}_{FE}^{I} \end{bmatrix}, \tag{49}$$

where the transformation mastrix $\mathbf{T}_{FE}$ has been defined on the finite element domain.

The conditions of continuity of the displacements and equilibrium of the tractions at the interface between the BE and FE domains are now satisfied by

$$\mathbf{U}^I_{ibed} = \mathbf{U}^I_{FE} = \mathbf{U}^I, \quad \mathbf{P}^I_{ibed} = -\mathbf{P}^I_{FE} = \mathbf{P}^I. \tag{50}$$

Thus, Equations (48) and (49) can be rearranged in the forms,

$$\begin{bmatrix} \mathbf{H}^{RR}_{ibed} & \mathbf{H}^{RI}_{ibed} & -\mathbf{G}^{RI}_{ibed} \\ \mathbf{H}^{IR}_{ibed} & \mathbf{H}^{II}_{ibed} & -\mathbf{G}^{II}_{ibed} \end{bmatrix} \begin{bmatrix} \mathbf{U}^R_{ibed} \\ \mathbf{U}^I \\ \mathbf{P}^I \end{bmatrix} = \begin{bmatrix} \mathbf{G}^{RR}_{ibed} \\ \mathbf{G}^{IR}_{ibed} \end{bmatrix} \left[\mathbf{P}^R_{ibed}\right], \tag{51}$$

$$\begin{bmatrix} \mathbf{K}^{RR}_{FE} & \mathbf{K}^{RI}_{FE} & \mathbf{T}^{RI}_{FE} \\ \mathbf{K}^{IR}_{FE} & \mathbf{K}^{II}_{FE} & \mathbf{T}^{II}_{FE} \end{bmatrix} \begin{bmatrix} \mathbf{U}^R_{FE} \\ \mathbf{U}^I \\ \mathbf{P}^I \end{bmatrix} = \begin{bmatrix} \mathbf{T}^{RR}_{FE} \\ \mathbf{T}^{IR}_{FE} \end{bmatrix} \left[\mathbf{P}^R_{FE}\right], \tag{52}$$

which may eventually be written together to form one single matrix equation,

$$\begin{bmatrix} \mathbf{H}^{RR}_{ibed} & \mathbf{H}^{RI}_{ibed} & -\mathbf{G}^{RI}_{ibed} & \mathbf{0} \\ \mathbf{H}^{IR}_{ibed} & \mathbf{H}^{II}_{ibed} & -\mathbf{G}^{II}_{ibed} & \mathbf{0} \\ \mathbf{0} & \mathbf{K}^{RR}_{FE} & \mathbf{K}^{RI}_{FE} & \mathbf{T}^{RI}_{FE} \\ \mathbf{0} & \mathbf{K}^{IR}_{FE} & \mathbf{K}^{II}_{FE} & \mathbf{T}^{II}_{FE} \end{bmatrix} \begin{bmatrix} \mathbf{U}^R_{ibed} \\ \mathbf{U}^I \\ \mathbf{P}^I \\ \mathbf{U}^R_{FE} \end{bmatrix} = \begin{bmatrix} \mathbf{G}^{RR}_{ibed} & \mathbf{0} \\ \mathbf{G}^{IR}_{ibed} & \mathbf{0} \\ \mathbf{0} & \mathbf{T}^{RR}_{FE} \\ \mathbf{0} & \mathbf{T}^{IR}_{FE} \end{bmatrix} \begin{bmatrix} \mathbf{P}^R_{ibed} \\ \mathbf{P}^R_{FE} \end{bmatrix}. \tag{53}$$

$$(N_F + N_B) \times (N_F + N_B) \qquad (N_F + N_B) \times (N^R_F + N^R_B)$$

The first column of matrices on the left hand side consists of terms from the BE domain only, the second and third column consist of terms for the interface part of both domains and the fourth column has terms which solely relate the displacements and tractions in the FE domain to one another. The dimensions of the matrices on the left and right hand sides of the equation are indicated using the symbolds N_F, N_B, N^R_F and N^R_B, to represent the number of degrees of freedom of the finite element domain, of the boundary element domain, of the non-interface part of the finite element domain and the non-interface part of the boundary element domain, respectively. If the tractions are known (notice that tractions may not be applied at the interface) Equation (53) may be solved to find the displacements.

3.3 Choice of Coupling Method

The equivalent BE matrix method has been developed for the case of coupling a single FE and single BE domain (Subsection 3.2). The complexity in implementing the method in a computer program is greater where an arbitrary number of boundary element domains is involved. So is the required effort in data preparation, since the interface and non-interface nodes of the FE and BE domains must be identified, and the matrices repartitioned to introduce each new domain.

The BE matrix method has the advantage over the FE matrix, or equivalent nodal forces, method that there is no matrix inversion involved in producing the global system of equations. This is the step (Equation (47)) which, for most practical problems, takes the greatest amount of computing time. Thus, for problems involving a single BE domain with almost as many degrees of freedom as the global system, the solution time may be doubled. The equivalent BE matrix method is therefore considerably more time efficient. However from Equation (53), it is seen that the equivalent BE matrix method requires more computer array storage space and thus is less memory efficient. It also carries the minor disbenefit that tractions cannot be applied at the interfaces of the domains.

No method has been developed here to solve the problem of discontinuous tractions in the BE coupling method. One way to overcome this problem is to define multiple coincident nodes where the discontinuities are present, hereby adding extra degrees of freedom to the global system of equations. Alternatively extra equations may be implemented to ensure equilibrium of the surface tractions.

For coupling with FE regions, extra terms would have to be derived. Mustoe [9] outlines four methods of dealing with this problem in two dimensions. This would add considerable complexity to the implementation of this method as well as its use. The method of expressing the BE matrices in terms of nodal forces on a finite element basis avoids having to allow for traction discontinuities at corners as well as at any point on smooth parts of the surface of the boundary element domains. In the numerical examples given in Section 4, it will be checked experimentally that this does not generate erroneous results compared to those obtained by a pure BE scheme where discontinuous tractions are allowed. The test is however confined to the analysis of a single boundary element domain.

Finally, a judgement also arises as to whether it is preferable to apply the loads in terms of tractions over finite areas of boundary element (or finite element) surfaces or if it is more convenient to specify the load in terms of nodal forces.

These reasons have contributed to the decision to implement the FE stiffness matrix approach of Subsection 3.1 rather than the BE matrix method described in Subsection 3.2.

3.4 Boundary Element Analysis of Problems with Geometrical Symmetry

Many problems of wave propagation through soil and solids involve structures and layered ground that have at least one plane of geometrical symmetry. Examples include tunnels, tracks and many types of foundations. When the geometry is symmetric the load and the corresponding response may, in any case, be split into a symmetric and an antisymmetric part. The total displacements may then be found as a linear combination of the displacements obtained by the two analyses involving, respectively:

1. symmetry of the load and response around the plane of geometric symmetry,

2. antisymmetry of the load and response around the plane of geometric symmetry.

Since the size of the system matrices depends on the number of degrees of freedom squared, the demand for computer memory is quartered when a symmetric description is used. Furthermore it is often much faster to make the two analyses for the reduced system than one analysis for the original (the full) system. Naturally, if the load is purely symmetric/antisymmetric the benefit from a symmetric description is even more pronounced.

In a finite element scheme only half the model needs to be analysed when a plane of symmetry exists. Usually the degrees of freedom which are known to be zero at the plane of symmetry are eliminated in the system of equations to satisfy the conditions at the interface between the modelled and the non-modelled part. Alternatively a very high stiffness (orders of magnitude higher than the average stiffness of the system) may be applied for those degrees of freedom so that the displacements here become insignificant relative to the displacements elsewhere. The second approach has the advantage that no reordering of the degrees of freedom is necessary. However, it is not physically correct, and mathematically the first method is more efficient.

The introduction of a plane of symmetry in a boundary element scheme is slightly more complicated than the implementation in a finite element scheme. One way to proceed is to discretize the plane of symmetry so that the conditions that apply here can be introduced in the same way as it is usually done in a FE scheme. However, this implies the introduction of degrees of freedom that are not present in the original model. Thus the results may be less accurate and, depending on the geometry of the model, there may be no or only a little net reduction of the number of unknowns in the system of equations. Especially, if a half-space is considered, only half the surface has to be discretized. However, the interface at the plane of symmetry has to be discretized a similar distance into the soil to obtain the same degree of accuracy in the model.

Instead, a method has to be developed where a discretization of the plane of symmetry is not necessary. For that purpose, consider the original BE system of equations for a single domain with identical, but mirrored discretizations of the surface on either side of the plane of geometrical symmetry $y = 0$,

$$\begin{bmatrix} \mathbf{H}^{++} & \mathbf{H}^{+-} \\ \mathbf{H}^{-+} & \mathbf{H}^{--} \end{bmatrix} \begin{bmatrix} \mathbf{U}^{+} \\ \mathbf{U}^{-} \end{bmatrix} = \begin{bmatrix} \mathbf{G}^{++} & \mathbf{G}^{+-} \\ \mathbf{G}^{-+} & \mathbf{G}^{--} \end{bmatrix} \begin{bmatrix} \mathbf{P}^{+} \\ \mathbf{P}^{-} \end{bmatrix}. \tag{54}$$

Superscripts $+$ and $-$ denote terms belonging to the half-spaces defined by $y > 0$ and $y < 0$, respectively. Subsequent superscripts $+-$, for instance, indicate the influence to degrees of freedom at $y > 0$ from degrees of freedom at $y < 0$. It is assumed that all sub-matrices are square (which disallows discontinuous tractions) and that $N/2$ nodes are located on either side of the plane of symmetry.

When the load, and thus also the response, is symmetric around the $y = 0$ plane, the following conditions apply for the displacements and the surface traction:

$$\begin{aligned} U_1(x,-y,z,\omega) &= U_1(x,y,z,\omega), & P_1(x,-y,z,\omega) &= P_1(x,y,z,\omega), \\ U_2(x,-y,z,\omega) &= -U_2(x,y,z,\omega), & P_2(x,-y,z,\omega) &= -P_2(x,y,z,\omega), \\ U_3(x,-y,z,\omega) &= U_3(x,y,z,\omega), & P_3(x,-y,z,\omega) &= P_3(x,y,z,\omega). \end{aligned} \tag{55}$$

Thus the displacements and tractions in the x and z directions are the same on both sides of the $y = 0$ plane of symmetry, whereas the y components are reflected. The degrees of freedom are now assumed to be ordered so that the 'mirror image' of degree of freedom j appears as degree of freedom $j + N/2$. Furthermore rows and columns are reordered so that all x degrees of freedom appear first, and all z degrees of freedom appear last on either side of the $y = 0$ plane. The arrays storing the displacements and tractions for the part of the model located at $y < 0$ may then be written as:

$$\mathbf{U}^- = \mathbf{R}_S \mathbf{U}^+, \quad \mathbf{P}^- = \mathbf{R}_S \mathbf{P}^+, \quad \mathbf{R}_S = \begin{bmatrix} \mathbf{I} & \mathbf{0} & \mathbf{0} \\ \mathbf{0} & -\mathbf{I} & \mathbf{0} \\ \mathbf{0} & \mathbf{0} & \mathbf{I} \end{bmatrix}. \tag{56}$$

Here $\mathbf{I}$ is the identity matrix with dimensions $(N/6 \times N/6)$ and $\mathbf{0}$ is the null matrix with the same dimensions. $\mathbf{R}_S$ is denoted *the reflection matrix* for symmetric load/response. In the case of antisymmetric load and response, the reflection matrix becomes

$$\mathbf{R}_A = \begin{bmatrix} -\mathbf{I} & \mathbf{0} & \mathbf{0} \\ \mathbf{0} & \mathbf{I} & \mathbf{0} \\ \mathbf{0} & \mathbf{0} & -\mathbf{I} \end{bmatrix} = -\mathbf{R}_S. \tag{57}$$

With the assumed order of the degrees of freedom, the original system of equations may eventually be reduced to:

$$\left(\mathbf{H}^{++} + \mathbf{R}\mathbf{H}^{+-}\right) \mathbf{U}^+ = \left(\mathbf{G}^{++} + \mathbf{R}\mathbf{G}^{+-}\right) \mathbf{P}^+. \tag{58}$$

The reflection matrix $\mathbf{R}$ is equal to $\mathbf{R}_S$ and $\mathbf{R}_A$ in case of symmetric and antisymmetric load and response, respectively, and only the first row of sub-matrices in Eq. (54) is taken into account. Thus the system of equations may be halved in size by 'adding' the contributions from the reflected part of the model to the part which is kept in the discretization.

In the present case only the part of the model present in the $y > 0$ half-space has to be modelled, and the following steps have to be carried out in the integration process:

1. The influence from integration points on the part of the surface at $y > 0$ to collocation points at $y > 0$ are found in the usual manner.

2. The influence from the 'mirror images' of the integration points to the collocation points are found by evaluating the same elements again, but with a change of sign on the y co-ordinates for the nodes. The contributions are then assembled into the existing system matrices.

Since the elements, and thus the local node order, will be mirrored in the process, a reordering of the nodes in each of the elements produced in this manner at $y < 0$ is necessary to ensure the correct direction of the normal vector. Alternatively, the model may be reduced to only include the part of the domain present at $y < 0$. In that case the reduced system is established from the second line of sub-matrices in Eq. (54). The reflection matrix remains the same.

So far it has been assumed that half of the nodes are present on either side of the plane of symmetry. This may be the case when constant elements are used, and is even possible with linear elements. However, when quadratic interpolation is used, some of the nodes will definitely have a y co-ordinate equal to zero when the discretization is strictly symmetric around the $y = 0$ plane. This leads to some numerical problems which will be discussed below.

For the nodes on the plane of symmetry the contributions from a node and its 'mirror image' are exactly the same. However, depending on the kind of symmetry, the sign on either the y degree of freedom or the x and the z degrees of freedom will be opposite. Since the contributions are added into *one* component in the **G** and **H** matrices, not stored separately (as they are in the original description), this eventually means that some of the rows in the reduced system matrices contain nothing but zeros. Notice that the diagonal term is zero, even if it only stores the influence from a single node, namely the node itself. The reason is that half the influence is obtained from one side of $y = 0$ and the other half is obtained by integration over elements on the other side of $y = 0$ to which the node also belongs. For the same reason, the contribution to other degrees of freedom will also be very small. The terms in the columns corresponding to the problematic degrees of freedom may even be zero if the other degree of freedom belongs to a node which is also on the plane of symmetry.

As explained in the previous subsection, it has been chosen to perform the solution in a finite element manner. Each boundary element domain is transformed into a macro finite element described by an equivalent stiffness matrix, the derivation of which involves an inversion of the **G** matrix. When some of the row contain nothing but zeros, the system is ill-conditioned. In theory, the inversion of such a system is impossible. However, due to the small errors introduced in the numerical integration, the terms in the problematic columns are not completely zero. Hence, a solution of the system of equations is still possible in practice; but the the solution algorithm is unstable and the results produced are erroneous unless the zero terms are in one or another way removed/avoided in the **G** matrix.

To obtain a stable system of equations, the following approaches may be suggested:

1. A certain amount of asymmetry is introduced so that the contributions from the original and the reflected elements are not exactly the same.

2. The rows and columns corresponding to the degrees of freedom which are known to be zero are eliminated.

It has been chosen to implement the second approach in the computer program BEASTS. The reasons are given below.

Ad. 1. One way of introducing asymmetry is to disregard some of the nodes or elements in the reflected part of the model. However the major problem is that some of the diagonal terms become zero. Since these terms are calculated entirely from the elements adjacent to the plane of symmetry, it is these elements (or the nodes of elements) that have to

be disregarded to avoid the problematic zeros in the diagonal of **G**. Just disregarding the elements/nodes in that are farthest away from the plane of symmetry, as it is common practice when the entire model is considered, will not stabilize the solution. Alternatively the asymmetry may be introduced in an arbitrary way, simply buy adding small numbers to the zeros terms in the **G** matrix. Mathematically this may be as good as leaving out elements or nodes in the reflected part of the domain. However, it is impossible to give any physical interpretation of the error which is introduced in this manner. The conclusion is that the first approach cannot be used, since the changes that are necessary to produce a stable system are conflicting with the initial assumption that the model should be symmetric (or antisymmetric) with respect to the y co-ordinate, at least in the vicinity of the $y = 0$ plane.

Ad. 2. The rows that contain zeros in all columns may be eliminated in the equivalent stiffness matrix. In this way the 'infinite' stiffness terms associated with the degrees of freedom that are known to be zero are avoided. However, even if the system of equations is, in this way, not badly scaled, erroneous results will still be produced. The reason is that the remaining stiffness terms for all other degrees of freedom are already determined inaccurately because the **G** matrix is not fit for inversion. Actually the inversion is only possible in the first place because a small numerical error has been introduced in the Gauss integration process. Therefore the reduction of the system must be applied before the matrix inversion. This implies a bit more bookkeeping, especially as it has to be ensured that the same degrees of freedom are removed from all sub-domains in the entire model. However this should not be a problem. Finally it should be noticed that when the degrees of freedom are removed before the matrix inversion, the calculation time may be reduced significantly if a large fraction of the nodes are on the plane of symmetry.

Hisatake *et al.* [4] proposed an alternative method which may be used to avoid an ill-conditioned matrix for inversion. Basically, their idea was to establish the equivalent stiffness matrix from the full system of equations, where the rows with nothing but zeros do not occur. However this requires the assembly of the double amount of terms in **G** and **H** and a matrix of the quadruple size has to be stored and inverted. Hence, the method suggested by Hisatake *et al.* is not as efficient as the second method, which has been proposed in this section and implemented in the computer program BEASTS [2].

The method of dealing with symmetric structures that has been developed in the present section may easily be generalized to the case where more than one plane of symmetry exist. Also, a formulation may be given where the plane of symmetry is placed arbitrarily. However, in most situations involving railway structures (which are the main consideration in the present project) only a single plane of symmetry may exist, and the track is most easily modelled with the centre line coinciding with one of the co-ordinate axes. It has therefore been chosen only to implement the facility to place a plane of symmetry at $y = 0$ in BEASTS.

4 Numerical Examples

In this section two numerical examples are given where the theory described in Sections 2 to 3 is tested against a semi-analytic solution. First, a homogeneous half-space is considered and a comparison is made not only with the semi-analytical solution but also the results obtained with a BE scheme where discontinuous tractions are allowed. Subsequently a half-space with a single layer of softer material on top is analysed.

4.1 Case 1: A Homogeneous Half-Space

A homogeneous, viscoelastic half-space is considered. The model has the parameters given in Table 1. These parameters correspond to sand with medium stiffness - here given in terms of the Young's modulus, E, and the Poisson Ratio, ν, which are related to the Lamé constants as

$$E = \frac{\mu\left(3\lambda + 2\mu\right)}{\lambda + \mu}, \quad \nu = \frac{\lambda}{2\left(\lambda + \mu\right)}. \tag{59}$$

The loss factor, η, defines a complex Young's modulus as $E^* = E\left(1 + i\eta\right)$, which again results in complex values of the Lamé constants and therefore also the phase velocities c_P and c_S. Notice that η is constant for all frequencies, well knowing that this results in a non-causal system in the time domain. However, the error due to the chosen damping model is very small.

Table 1. Parameters for homogeneous half-space.

Layer	E [MPa]	ν	ρ [kg/m^3]	η	Depth [m]
1	369	0.257	1550	0.10	Half-space

A harmonic, uniformly distributed vertical excitation is applied on the surface of the half-space over an area of 3×3 m^3. The analysis is carried out for the three frequencies 10 Hz, 20 Hz and 40 Hz. The following models are used for comparison:

1. A semi-analytic solution based on Fast Fourier Transforms (FFT) - inverse FFT with 2048 points per 500 metres in the x and y directions and an analytical solution in the z direction, *i.e.* over the depth. See Reference [10] for further explanation.

2. A boundary element solution based on the original formulation for a single BE domain, Equation (33), where discontinuous tractions are allowed.

3. A boundary element formulation in the macro finite element sense. The results are calculated using the computer program BEASTS described in Reference [2].

In neither the first nor the second solution has any use been made of the symmetry. However, in the third solution, symmetry around the $x-z$ plane has been utilized, see the input file for BEASTS in Appendix A. The vertical load is applied in terms of surface traction over the

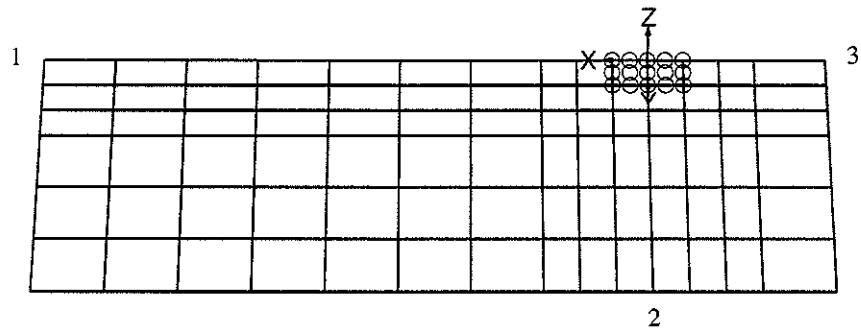

Figure 6. Mesh used for boundary element analysis of the homogeneous half-space.

3×3 m^3 area with the amplitude $1/9$ Pa in the first two cases. In the third case the load is applied as point forces adding up to a total of 1 N and distributed according to the shape functions as defined by Equation (45). Hence, the total intensity of the load is the same in all the models.

For all frequencies the elements in the BE discretization have the dimensions 1.5×1.5 m^2 in the vicinity of the area, where the load is applied. Farther away from the area of excitation the length of the elements is doubled. The mesh is illustrated in Figure 6. For the original BE formulation with discontinuous tractions a mesh with double the size is used with the other half of the elements present in the negative y half-space.

The influence of the distance from the load to the edge, where the surface of the half-space is artificially truncated, is studied. Thus, as shown on Figure 6, the mesh does not extend the same distance away from the load in all directions. In the Figures 7 to 12 the results obtained with the different models have been plotted. The absolute values of the displacement amplitudes and the phase shift are shown as functions of the distance r from the centre point of the loaded area, which coincides with origin of the coordinate system. Figures 7, 9 and 11 show the vertical displacements, whereas Figures 8, 10 and 12 contain results for the horizontal displacements.

Results obtained with the semi-analytic solution are plotted in red, dotted lines ($\cdots$). Results from the original BE solution, *i.e.* method 2, are plotted in blue. The dots ($\cdot$) refer to results obtained along the line between origin and 1 on Figure 6, triangles ($\triangle$) refer to the line ranging between origin and point 2, and crosses ($+$) refer to results along the line towards point 3. For the FE based BE solution the corresponding solutions are plotted in green using the symbols ($\circ$), ($\triangledown$) and ($\times$), respectively. The following observations can be made:

- The two BE models produce results that are almost identical except for some minor discrepancies in a small region near the centre of the loaded area. The 'errors' in the FE based boundary element solution arise because of the lacking ability to apply discontinuous tractions. However, the effect is local and farther away from the load the influence of the discontinuity of the surface traction is vanishing.

- Both BE solutions are in good accordance with the semi-analytic solution. This counts for both the amplitude and the phase shift.

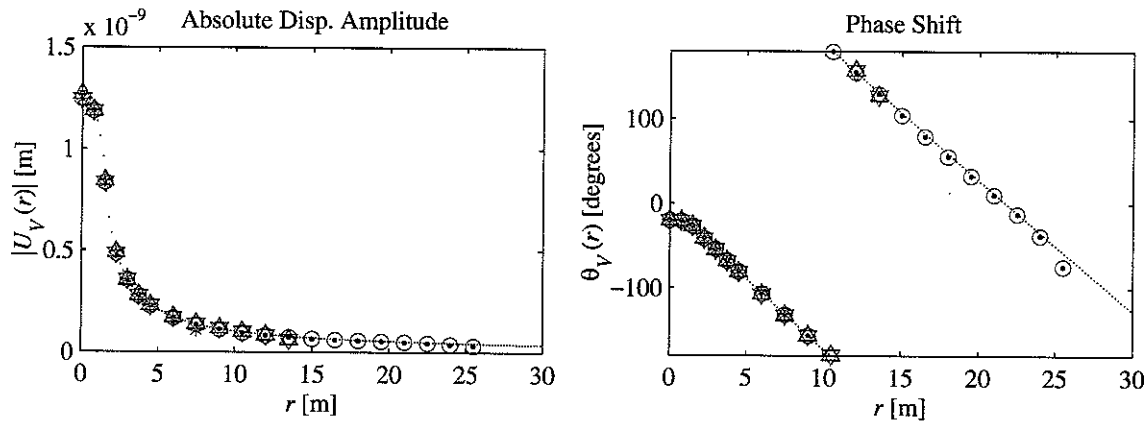

Figure 7. Comparison of two different BE models with semi-analytical solution for a homogeneous half-space: Vertical surface displacements for the frequency 10 Hz.

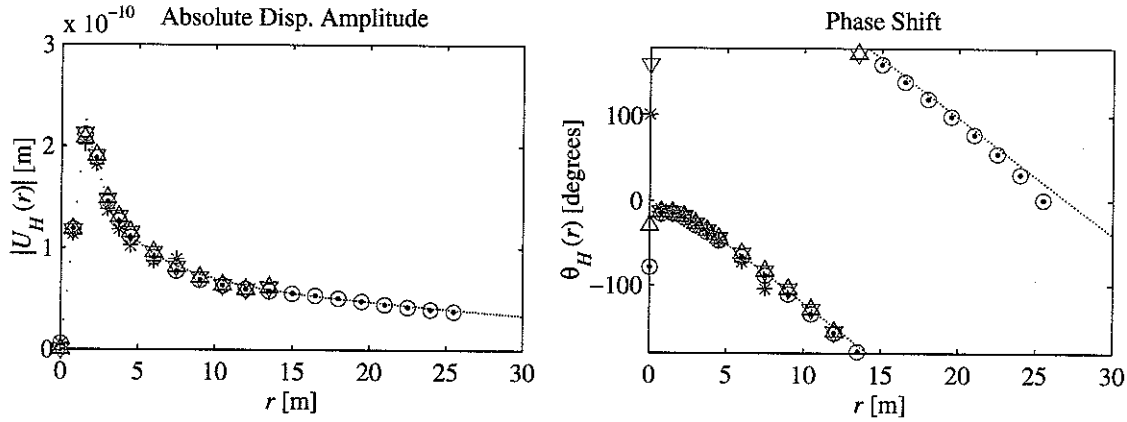

Figure 8. Comparison of two different BE models with semi-analytical solution for a homogeneous half-space: Horizontal surface displacements for the frequency 10 Hz.

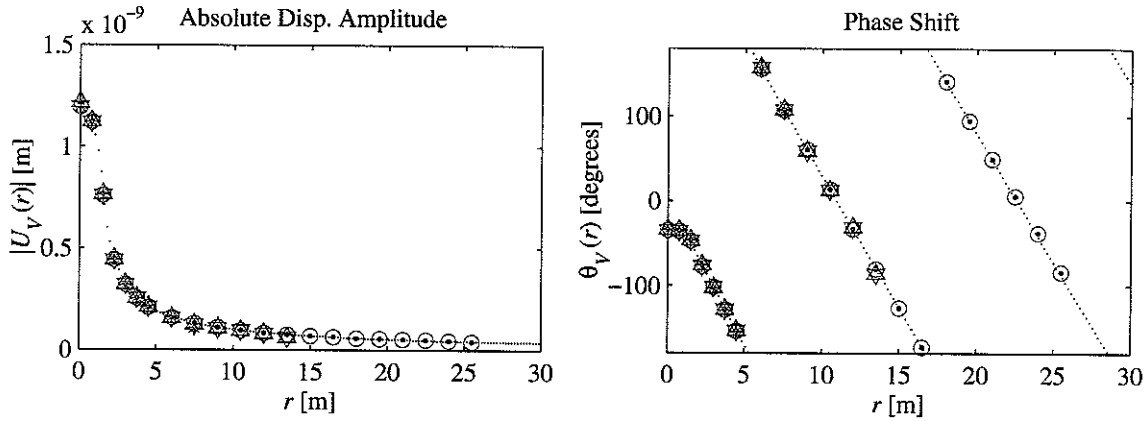

Figure 9. Comparison of two different BE models with semi-analytical solution for a homogeneous half-space: Vertical surface displacements for the frequency 20 Hz.

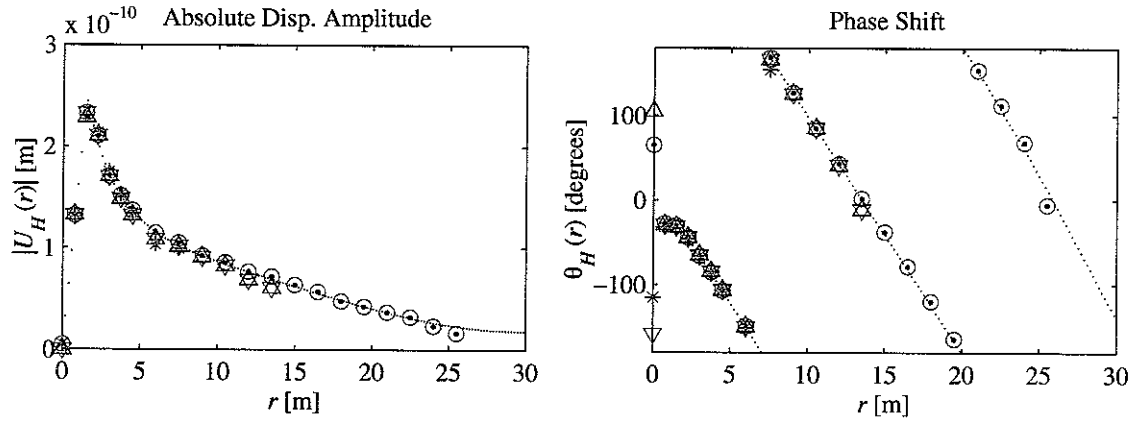

Figure 10. Comparison of two different BE models with semi-analytical solution for a homogeneous half-space: Horizontal surface displacements for the frequency 20 Hz.

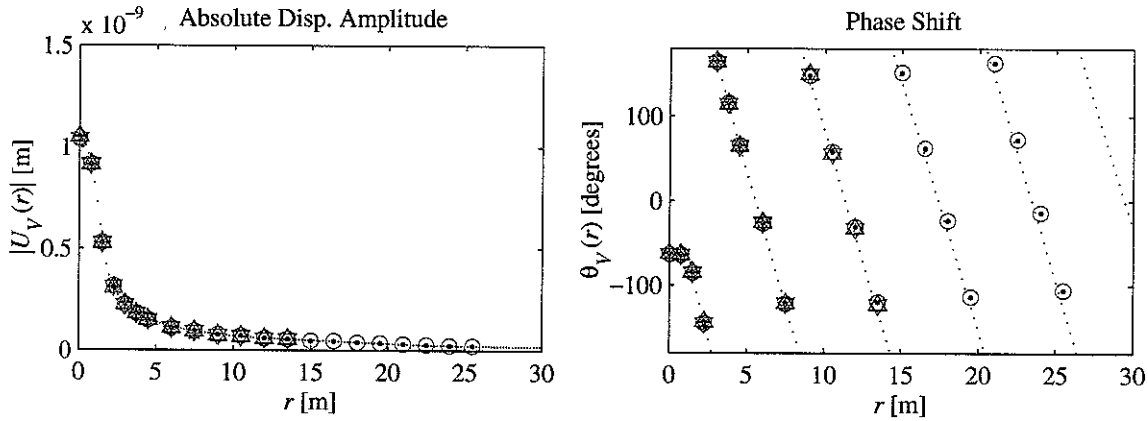

Figure 11. Comparison of two different BE models with semi-analytical solution for a homogeneous half-space: Vertical surface displacements for the frequency 40 Hz.

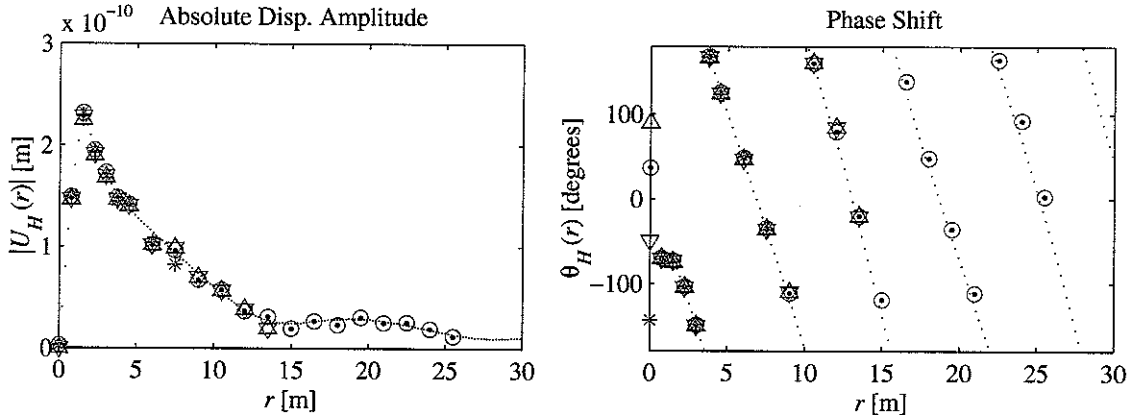

Figure 12. Comparison of two different BE models with semi-analytical solution for a homogeneous half-space: Horizontal surface displacements for the frequency 40 Hz.

- The distance from the load to the edge of the mesh has no, or little, effect on the precision of the BE results close to the loaded area. Even close to the edge, the results are useful. The reason is likely to be the small impedance mismatch between a half-space and a full-space.
- The agreement of the BE results with the semi-analytical solution is better for the 'low' frequencies (10 Hz, 20 Hz) than for the 'high' frequency (40 Hz). This is due to a combination of two reasons: the influence of the edge is insignificant and the elements are not sufficiently small for frequencies much above 30 Hz. Thus, for the $f = 40$ Hz only *two* elements are available per Rayleigh wave length. The fact that the results are still quite satisfactory at 40 Hz indicates that the BEM with quadratic interpolation is very powerful and provides good results, even when extremely few elements are used in the discretization.

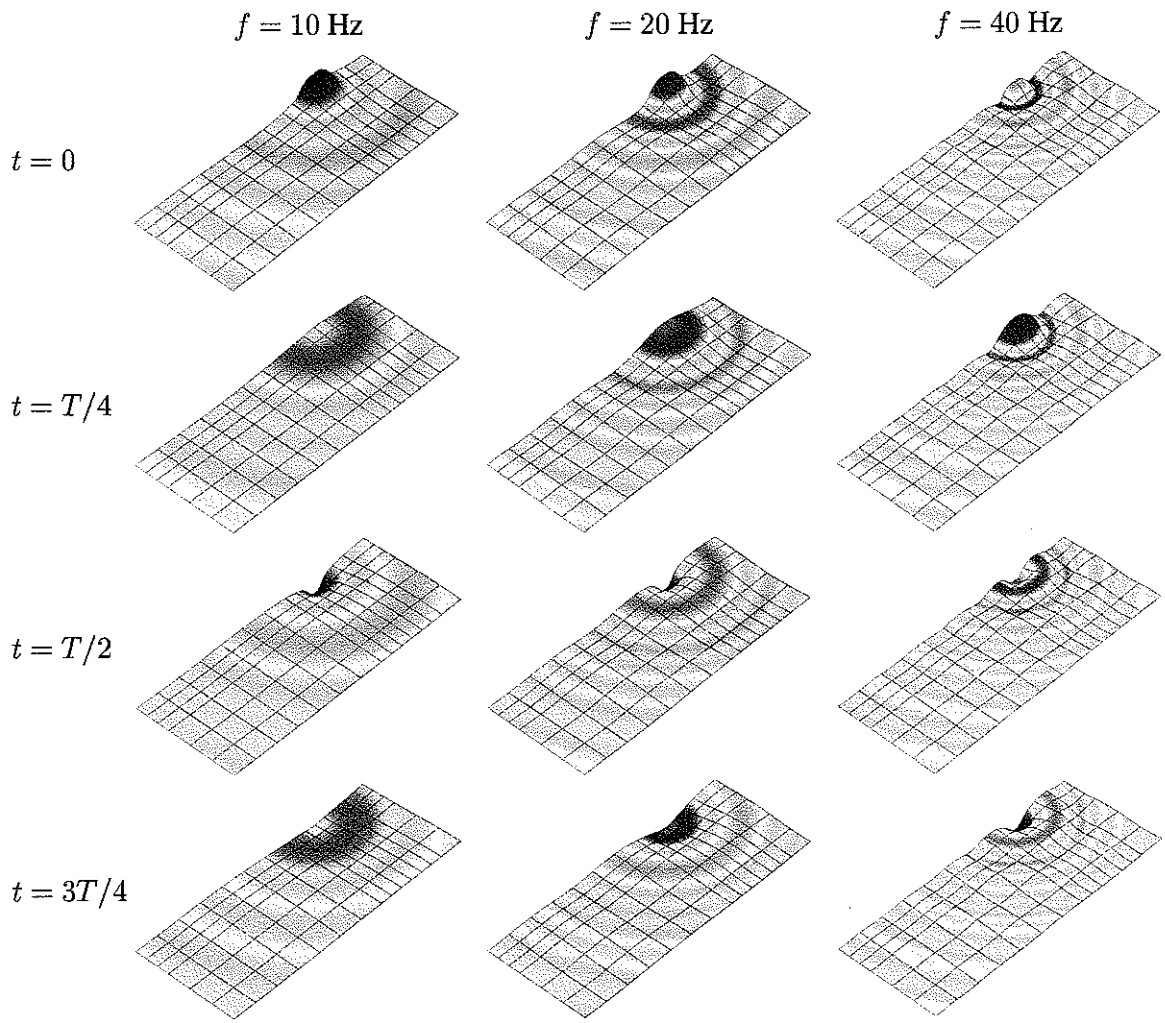

Figure 13. Surface displacement of the homogeneous half-space. Red and blue colours indicate positive and negative vertical displacements, respectively, and parts of the surface with near-zero vertical displacement are in shades of green.

The wave propagation on the surface of the half-space, *i.e.* the Rayleigh waves, are illustrated on Figure 13. The displacements are plotted for four time steps during a single period of time, $T = 1/f$, given a harmonic excitation with the exponential term $e^{i\omega t}$.

4.2 Case 2: A Single Viscoelastic Layer over a Half-Space

A viscoelastic, horizontal layer of soft clay and with a depth of 2 metres is overlaying a homogeneous half-space of a stiffer clay. The two soil materials have the parameters listed in Table 2. As the soil in the top layer is softer than the soil underneath, a cut-off frequency, f_0, exists below which only evanescent waves are present. However, when the excitation frequency goes beyond f_0 travelling waves will propagate through the layer.

Table 2. Parameters for layered half-space.

Layer	E [MPa]	ν	ρ [kg/m^3]	η	Depth [m]
1	60	0.44	1500	0.10	2.0
2	360	0.49	2000	0.10	Half-space

The same analysis that was carried out for the homogeneous half-space is performed for the layered half-space. Thus, a harmonic, vertical excitation is applied on the surface over and area of 3×3 m^2. Again the frequencies 10 Hz, 20 Hz and 40 Hz are considered. However, only the semi-analytic solution scheme and the BE method based on finite element coupling are compared as no means of coupling two sub-domains in a boundary element sense has been implemented in BEASTS. Therefore the second approach listed in the previous subsection has not been taken in the present example.

For the first method, *i.e.* the semi-analytic solution, the same discretization used in the FFT-iFFT of the surface in Subsection 4.1 has been used for both the surface and the interface between the layer and the half-space. Likewise, a BE mesh identical to the one shown on Figure 6 has been used for both the surface and the interface, see the input file for BEASTS in Appendix B. It should be noted that this actually results in a distance between two boundaries that is only two thirds of the element length for most parts of the BE model.

The results obtained with the semi-analytic solution and the boundary element scheme are shown on Figures 14 to 19. Red, dotted lines ($\cdots$) are the semi-analytic solutions, whereas green circles ($\circ$), triangles ($\triangledown$) and crosses ($\times$) indicate the results from the BE scheme along the lines on the surface between origo and the points 1, 2 and 3 on Figure 6, respectively. It is noticed that:

- At 10 Hz travelling waves do not propagate through the top layer. Five metres away from the source $|U_V(r)|$ has decreased to less than 10% of the value at the centre of the loaded area and the phase shift is clearly not a piece-wise linear function of the distance r.
- For the frequencies higher than 10 Hz, travelling waves occur in the viscoelastic layer. Here the excitation frequency is higher than the cut-off frequency.

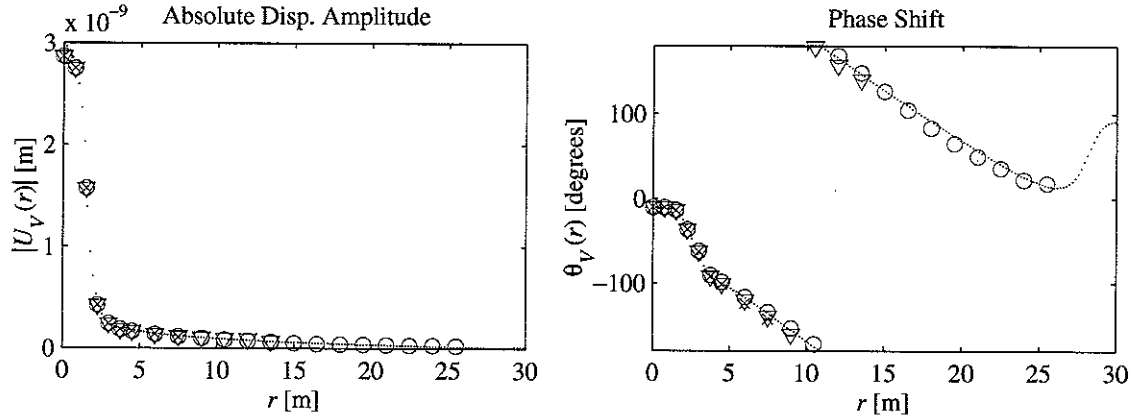

Figure 14. Comparison of BE model with semi-analytical solution for a layered half-space: Vertical surface displacements for the frequency 10 Hz.

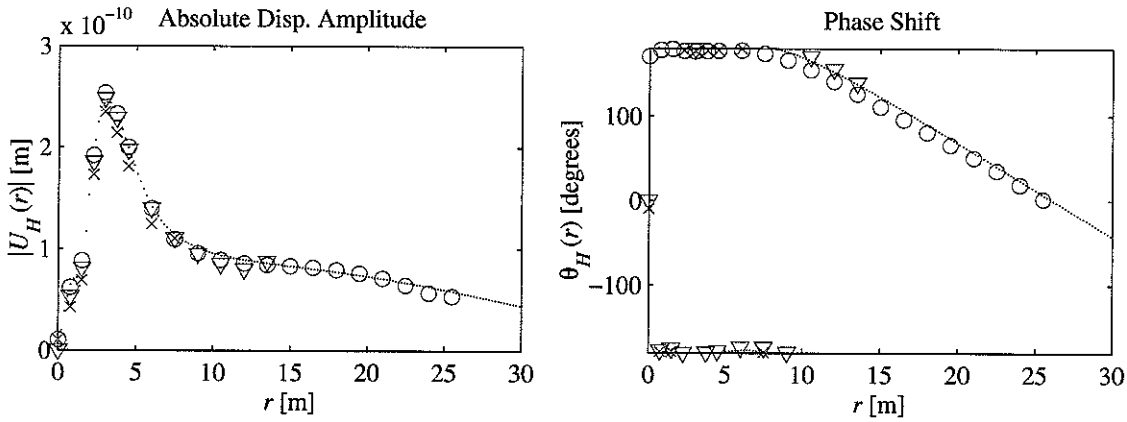

Figure 15. Comparison of BE model with semi-analytical solution for a layered half-space: Horizontal surface displacements for the frequency 10 Hz.

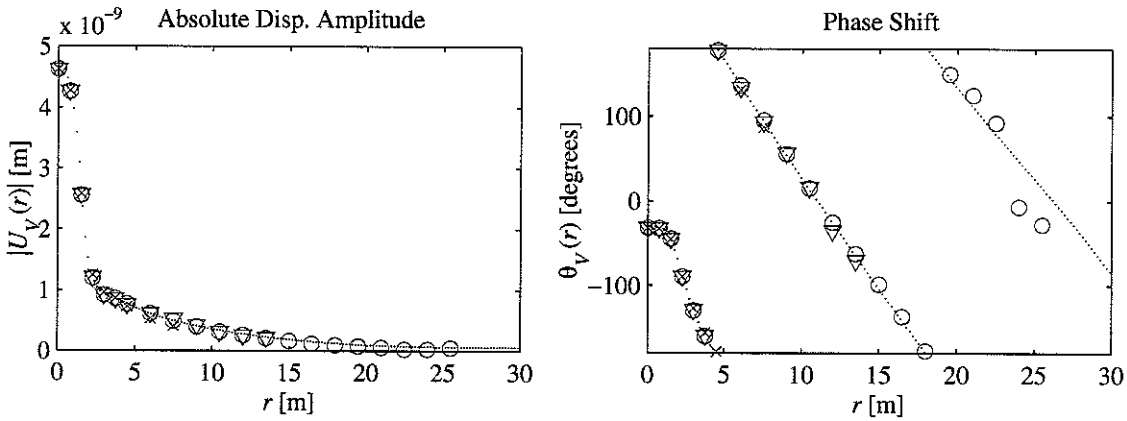

Figure 16. Comparison of BE model with semi-analytical solution for a layered half-space: Vertical surface displacements for the frequency 20 Hz.

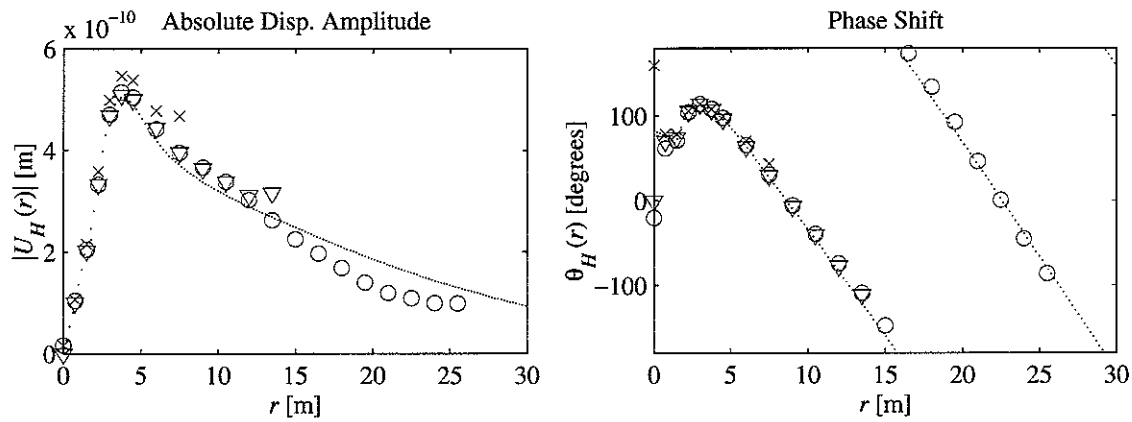

Figure 17. Comparison of BE model with semi-analytical solution for a layered half-space: Horizontal surface displacements for the frequency 20 Hz.

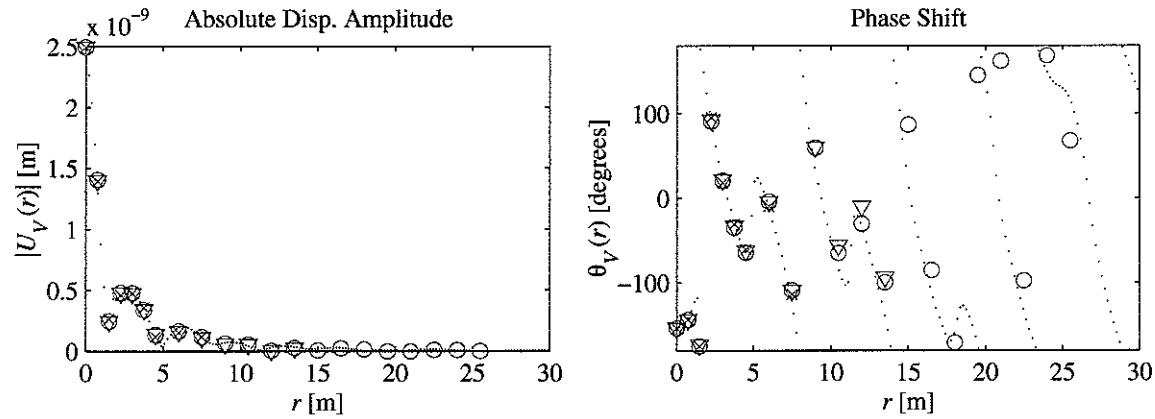

Figure 18. Comparison of BE model with semi-analytical solution for a layered half-space: Vertical surface displacements for the frequency 40 Hz.

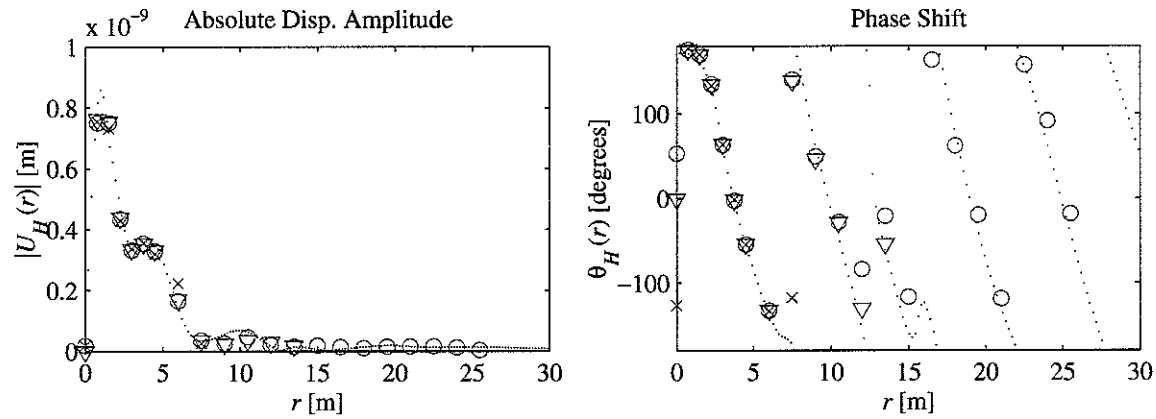

Figure 19. Comparison of BE model with semi-analytical solution for a layered half-space: Horizontal surface displacements for the frequency 40 Hz.

- The influence of the edge is much more pronounced than it is in the example with the homogeneous half-space. This is partly due to the fact that the impedance mismatch between the modelled layer and the 'full-space' that lies beyond the edge is much higher than that between the homogeneous half-space and the 'full-space'.

- A better discretization is needed for the layered half-space than for the homogeneous half-space. Thus the BE mesh used in the present analysis is not sufficiently detailed to give a satisfactory result at 40 Hz. The semi-analytical solution indicates that the wave propagation pattern is quite complex, *i.e.* the wave lengths change with the distance from the source (the phase shift is not a piece-wise linear function of r).

Hence it may be concluded that for a layered medium or structures coupled with soil, where complicated wave propagation patterns may occur, a bigger and more refined mesh has to be used than is necessary for a homogeneous half-space.

5 Conclusions

The theory for a multi-domain boundary element scheme has been formulated for analysis of harmonic vibration wave propagation through three-dimensional, viscoelastic media. The subdomains may be either open or closed and may be arbitrarily shaped. Thus the scheme is useful for the analysis of structure-soil interaction problems. The coupling between the individual subdomains is established by a transformation of the BE domains into equivalent macro elements, which are assembled in the finite element sense. Hence a further coupling with finite elements is straight forward.

Numerical examples are given for the wave propagation due to a surface excitation of a homogeneous and a layered half-space. Generally the analyses show that fairly accurate results are obtained with very few elements per wave length. Hence, the scheme may be used for the analysis of problems with more complicated geometries, even at frequencies which are of interest in such topics as railway tunnel engineering. An example analysis of a bored tunnel may be found in Reference [2], where documentation is provided for the computer program BEASTS that is based on the BE formulation given in the present report.

Acknowledgement

L. Andersen would like to thank the Danish Technical Research Council for financial support via the research project: 'Damping Mechanisms in Dynamics of Structures and Materials'.

References

[1] S. Ahmad and P.K. Banerjee. Multi-domain BEM for two-dimansional problems of elastodynamics. *Int.J.Num.Meth.Eng.*, 26:891–911, 1988.

[2] L. Andersen and C.J.C. Jones. BEASTS - A Computer Program for Boundary Element Analysis of Soil and Three-dimensional Structures. ISVR Technical Memorandum 868, Institute of Sound and Vibration Research, University of Southampton, Southampton SO17 1BJ, England, October 2001.

[3] J. Dominguez. *Boundary elements in dynamics.* Computational Mechanics Publications, Southampton, 1993.

[4] M. Hisatake, T. Ito, and H. Ueda. Three dimensional symmetric coupling of boundary and finite element methods. In *Boundary Elements. Proceedings of the Fifth International Conference.* Ed. C.A. Brebbia, T. Futagami and M. Tanaka, pages 985–994, 1983.

[5] C.J.C. Jones and D.J. Thompson. A boundary Element Model for Two-Dimensional Elastodynamics on a Single Open or Closed Domain. ISVR Technical Memorandum 838, Institute of Sound and Vibration Research, University of Southampton, Southampton SO17 1BJ, England, May 1999.

[6] C.J.C. Jones, D.J. Thompson, and M. Petyt. Ground-Borne Vibration and Noise from Trains: Elastodynamic Analysis Using the Combined Boundary Element and Finite Element Methods. ISVR Technical Memorandum 844, Institute of Sound and Vibration Research, University of Southampton, Southampton SO17 1BJ, England, October 1999.

[7] C.J.C. Jones, D.J. Thompson, and M. Petyt. TEA - A Suite of Computer Programs for Elastoydnamic Analysis Using Coupled Boundary Elements and Finite elements. ISVR Technical Memorandum 840, Institute of Sound and Vibration Research, University of Southampton, Southampton SO17 1BJ, England, August 1999.

[8] J.C. Lachat. *A Further Development of the Boundary Integral Technique for Elastostatics.* PhD thesis, University of Southampton, United Kingdom, 1975.

[9] G.G.W. Mustoe. *A combination of the finite element and boundary integral procedures.* PhD thesis, Swansea University, United Kingdom, 1980.

[10] X. Sheng, C.J.C. Jones, and M. Petyt. Ground vibration generated by a harmonic load acting on a railway track. *J. Sound Vib.*, 225(1):3–28, 1999.

[11] O. Tullberg and L. Bolteus. A critical study of different boundary element stiffness matrices. In *Boundary Element Methods in Engineering*, Ed. C.A. Brebbia, pages 625–635, 1982.

A BEASTS Input: Homogeneous Half-Space

This is the input file for the computer program BEASTS used for the boundary element analysis of the homogeneous half-space in Subsection 4.1. An explanation for the commands used and the general layout of the file is given in Reference [2].

```
*Title

A Homogeneous Half-Space, LA, 15/8/2001

C This is an example file for use with the BE program BEASTS

*Material Properties

  269000000  0.257  1550.0  0.1000

*multi file output

*plane of symmetry

*Frequencies

  10.000
  20.000
  40.000

*Node coordinates

   -10.50   0.00   0.00 ! 1

 +offset nodes
      1     1     1.50     0.00     0.00     4 ! 2 to 5

 +offset nodes
      5     5     0.75     0.00     0.00    12 ! 6 to 17

 +offset nodes
     17    17     1.50     0.00     0.00    16 ! 18 to 33

 +offset nodes
      1    33     0.00     0.75     0.00     6 ! 34 to 231

 +offset nodes
    199   231     0.00     1.50     0.00     8 ! 232 to 495
```

```
*Boundary Element Domain 1

      1 ! Material Properties Set 1

      1     2     3    36    69    68    67    34    35

 +copy
      1     1     2    15

 +copy
      1    16    66     6

*Loads

      9   0.000   0.000   0.000   0.000   0.0138889   0.000
     42   0.000   0.000   0.000   0.000   0.0555556   0.000
     75   0.000   0.000   0.000   0.000   0.0138889   0.000

     10   0.000   0.000   0.000   0.000   0.0555556   0.000
     43   0.000   0.000   0.000   0.000   0.2222222   0.000
     76   0.000   0.000   0.000   0.000   0.0555556   0.000

     11   0.000   0.000   0.000   0.000   0.0277778   0.000
     44   0.000   0.000   0.000   0.000   0.1111111   0.000
     77   0.000   0.000   0.000   0.000   0.0277778   0.000

     12   0.000   0.000   0.000   0.000   0.0555556   0.000
     45   0.000   0.000   0.000   0.000   0.2222222   0.000
     78   0.000   0.000   0.000   0.000   0.0555556   0.000

     13   0.000   0.000   0.000   0.000   0.0138889   0.000
     46   0.000   0.000   0.000   0.000   0.0555556   0.000
     79   0.000   0.000   0.000   0.000   0.0138889   0.000

*End
```

B BEASTS Input: Layered Half-Space

This is the input file for the computer program BEASTS used for the boundary element analysis of the layered half-space in Subsection 4.2. An explanation for the commands used and the general layout of the file is given in Reference [2].

```
*Title

A Layered Half-Space, LA, 15/8/2001

C This is an example file for use with the BE program BEASTS

*Material Properties

   60E6  0.44  1500.0  0.1000
  360E6  0.49  2000.0  0.1000

*multi file output

*plane of symmetry

*Frequencies

  10.000
  20.000
  40.000

*Node coordinates

   -10.50   0.00   0.00 ! 1

 +offset nodes
      1     1     1.50     0.00     0.00     4 ! 2 to 5

 +offset nodes
      5     5     0.75     0.00     0.00    12 ! 6 to 17

 +offset nodes
     17    17     1.50     0.00     0.00    16 ! 18 to 33

 +offset nodes
      1    33     0.00     0.75     0.00     6 ! 34 to 231

 +offset nodes
    199   231     0.00     1.50     0.00     8 ! 232 to 495

 +offset nodes
      1   495     0.00     0.00    -2.00     1 ! 496 to 990
```

```
*Boundary Element Domain 1

      1 ! Material Properties Set 1

      1     2     3    36    69    68    67    34    35

 +copy
      1     1     2    15

 +copy
      1    16    66     6

 +mirror copy
      1   112   495

*Boundary Element Domain 2

      2 ! Material Properties Set 2

    496   497   498   531   564   563   562  529   530

 +copy
      1     1     2    15

 +copy
      1    16    66     6

*Loads

      9    0.000    0.000    0.000    0.000    0.0138889    0.000
     42    0.000    0.000    0.000    0.000    0.0555556    0.000
     75    0.000    0.000    0.000    0.000    0.0138889    0.000

     10    0.000    0.000    0.000    0.000    0.0555556    0.000
     43    0.000    0.000    0.000    0.000    0.2222222    0.000
     76    0.000    0.000    0.000    0.000    0.0555556    0.000

     11    0.000    0.000    0.000    0.000    0.0277778    0.000
     44    0.000    0.000    0.000    0.000    0.1111111    0.000
     77    0.000    0.000    0.000    0.000    0.0277778    0.000

     12    0.000    0.000    0.000    0.000    0.0555556    0.000
     45    0.000    0.000    0.000    0.000    0.2222222    0.000
     78    0.000    0.000    0.000    0.000    0.0555556    0.000

     13    0.000    0.000    0.000    0.000    0.0138889    0.000
     46    0.000    0.000    0.000    0.000    0.0555556    0.000
     79    0.000    0.000    0.000    0.000    0.0138889    0.000

*End
```